Rock Mechanics Bulletin 5 (2026) 100235

Contents lists available at ScienceDirect

Rock Mechanics Bulletin

journal homepage: www.keaipublishing.com/en/journals/rock-mechanics-bulletin

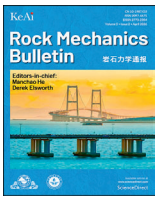

Full Length Article

Integration of image and dipole sonic logs for identification of natural fractures and stress-induced anisotropy in Asmari reservoir (A case study, SW Iran)

Maziar Torkaman [a], Soheila Bagheri [b,*], Mahdi Rastegarnia [c]

[a] Wireline Logging Department, Weatherford, Saskatchewan, Canada
[b] Petroleum Engineering Department, Sarvak-Azar Engineering & Development Company, Tehran, Iran
[c] Geoscience Department, Dashte Azadegan Arvand Oil and Gas Development Company, Tehran, Iran

ARTICLE INFO

Keywords:
Anisotropy
Dispersion analysis
Dipole-sonic image
Stress analysis
Qaleh-Nar oilfield

ABSTRACT

Borehole sonic dispersion analysis is a technique that provides valuable insights into the realm of borehole sonic interpretation. This research involves an analysis of shear-wave anisotropy and ultrasonic image logs to differentiate between types of fractures and their orientations. Evaluating fractures relies on core samples and image logs are limited. This highlights the need for a more affordable and efficient way to analyse fractures. A challenge in the wellbore is distinguishing natural fractures from those caused by drilling. Using oil-based mud often makes it hard to find signs indicating the direction of in-situ stress. A new method has been created to reliably identify natural fractures when image logs are insufficient for mapping fracture networks. The cross-dipole data reveals five main zones exhibiting shear-wave splitting. Higher anisotropy is observed at shallower depths, while the deeper interval shows low porosity accompanied by considerable inhomogeneity, highlighting potential areas of concern. The dominant directions of anisotropy are aligned with NW-SE, WNW-ESE, and N-S orientations. Slowness frequency analysis of rotated flexural waves identifies fracture types. Dispersion profiles show natural and induced fractures, with cross-over patterns indicating stress-induced anisotropy. Significant inhomogeneity is observed in the bottom interval, where the differences between maximum and minimum energy level are pronounced. Wider dispersion curves suggest breakouts are slowing high-frequency flexural waves, indicating mechanical damage. The maximum stress direction is determined by the fast-shear azimuth. In conclusion, this study demonstrates that by integrating acoustic shear dispersion, shear anisotropy, Stoneley analysis, and image log data, fractures within the borehole wall can be effectively investigated.

1. Introduction

Borehole acoustic logging is recognized as one of the most efficient and reliable methods for measuring the elastic properties of subsurface rock (Lei et al., 2021; Mao, 1987). Modern dipole sonic logging tools, such as the Dipole Sonic Imager (DSI), can measure shear waves in both fast and slow formations and can quantify shear anisotropy within the surrounding rock (Esmersoy et al., 1995; Mueller et al., 1994). Insights into anisotropy provide valuable information that complements interpretations of lithofacies, poro-permeability, and seismic dataset in heterogeneous reservoirs (Wood, 2024). Acoustic anisotropy may arise from mechanical anisotropy, fractures, or stress variations.

Cross-dipole logging, aided by advanced frequency domain processing, has proven to be a valuable technique for characterizing the mechanical state of the rock formation around the borehole (Plona et al., 2006). Slowness-dispersion analysis enables the identification of stress-induced azimuthal anisotropy. When it is confirmed that anisotropy results from differential stress, it becomes possible to determine the direction of maximum horizontal stress based on the orientation of fast shear waves in a near-vertical wellbore (Ellis and Singer, 2007; Sinha and Kostek, 1996; Tang et al., 1999, 2002; Winkler et al., 1998). This method is commonly used in the petroleum industry to complement other techniques, such as borehole failure assessments from caliper logs and imaging, to deduce the direction and magnitude of present-day horizontal stresses.

Analysing dispersion curves has been shown to identify radial

* Corresponding author.
E-mail address: Bagheri.soheila@gmail.com (S. Bagheri).
Peer review under the responsibility of Chinese Society for Rock Mechanics & Engineering.

https://doi.org/10.1016/j.rockmb.2025.100235
Received 26 April 2025; Received in revised form 30 June 2025; Accepted 6 August 2025
Available online 21 August 2025

gradients of shear slowness associated with mechanical damage in the formation (Sinha et al., 2008). The dispersion analysis of flexural waves in a dipole sonic log can reveal important characteristics such as anisotropy, shear velocity, and the presence of fractures in the formations adjacent to the borehole (Irofti et al., 2023). Recently, it has been demonstrated that frequency-domain processing of cross-dipole data (slowness-frequency or dispersion analysis) can differentiate between intrinsic anisotropy (i.e. bedding, shales, and aligned fractures) and stress-induced anisotropy (Fang et al., 2015). This frequency-domain processing enhances traditional time-based semblance processing, providing a more comprehensive description of the formation (Plona et al., 2006). By integrating this technique with image logs, the fractures can be differentiated as either open or closed (Irofti et al., 2023).

Well-established measurement techniques, such as oriented four-arm caliper data and borehole imaging data (including Formation Micro Imager (FMI), Oil-Based Micro Imager (OBMI), and Ultrasonic Borehole Imager (UBI)), have been extensively utilized to detect and quantify the distributions, orientations, and forms of fractures at high resolution. These measurements also help relate borehole elongation, shape, and failure to the direction of in-situ horizontal stresses (Plumb and Hickman, 1985; Zoback et al., 1985). In vertical wells, the elongation direction of the borehole corresponds to the direction of minimum horizontal stress. Additionally, observing stress-induced wellbore breakouts is an effective method for determining in-situ stress orientation in wells (Wang et al., 2022).

The drilling-induced fractures in vertical wells occur when wellbore pressure (mud weight) exceeds the stress concentration necessary to create a tensile fracture (Plumb and Hickman, 1985; Zoback, 2007). In some situations, when the current stress aligns similarly with the paleo-stress, it becomes challenging to distinguish between natural fractures and drilling-induced fractures (Al-Adani and Alkhatib, 2009). For instance, the orientation of many observed fractures often resembles the drilling-induced fractures that form due to tensile failure near the borehole, which is parallel to the in-situ principal stress. In these cases, cross-dipole sonic logging provides more accurate results (Al-Adani and Alkhatib, 2009).

Methods for characterizing stress that depend on observing borehole failure through images are limited to boreholes that show signs of failure. In contrast, acoustic technologies allow for the analysis of the likelihood that these failure features extend into the surrounding formation (Al-Adani and Alkhatib, 2009). Additionally, there are cases where high differential stresses are noted due to borehole failure, yet there is a lack of shear wave anisotropy (Donald et al., 2015).

In this paper, we employed slowness-dispersion analysis to identify the primary source of anisotropy and subsequently compared these findings with observations from Ultrasonic Images. When both methods confirm a particular feature, the likelihood of its presence in the formation increases. However, for non-planar features, like microfractures, which do not establish any plane of symmetry in the formation, the acoustic anisotropy will remain unaffected. Additionally, when the aperture of microfractures is smaller than the resolution of the borehole image, those fractures will not be detectable. In this case, the Stoneley wave is analyzed to detect borehole fluid mobility into the formation. Then, by comparing with the porosity profile, Stoneley will help indicate the presence of microfractures (Al-Adani and Alkhatib, 2009).

A thorough investigation of aligned fractures is crucial for enhancing hydrocarbon production. Understanding formation stresses can significantly assist in planning stimulation treatments and predicting sand production along with borehole stability. Therefore, it is important to differentiate between stress-induced anisotropy and the structural or intrinsic anisotropy of the formation (Winkler et al., 1998).

The primary objectives of this study are to examine fracture and stress-induced sonic anisotropy using a combination of image (UBI/OBMI) and Dipole sonic logs in the Qaleh-Nar Oilfield, allowing for the investigation of fractures beyond the borehole wall.

2. Geological setting

The Qaleh Nar anticline is an asymmetric anticline located in the northern part of the Dezful Embayment, where the fractured Asmari carbonate serves as the primary reservoir rock (Habibnia et al., 2021). The Qaleh Nar oilfield is a crucial site in the northernmost region of the Dezful Embayment (Fig. 1). Since 1975, operations at this oilfield have focused on the fractured carbonates of the Oligo-Miocene Asmari Formation, which has been drilled at 11 different wells (Motiei, 1995). At the Asmari level, the Qaleh Nar anticline forms an asymmetric fold measuring approximately 3×18 km, with a WNW-trending hinge line and two prominent culminations (Motiei, 1995; Razavi Pash, 2020). The underground contour map of the Asmari reservoir reveals several faults within the studied oilfield (Fig. 1). However, the impact of these faults on the continuity of the Asmari reservoir has yet to be investigated.

The Asmari Formation (Oligocene to the Early Miocene), is widespread throughout the Zagros Basin but is most prominently developed in the Dezful Embayment. In the Qaleh-Nar Oilfield, the Asmari Formation consists of shallow marine limestones, dolomitic limestones, and argillaceous limestones, making it a typical example of a fractured carbonate reservoir (Rezaeeparto et al., 2024). In the study area, the lower boundary of the Asmari Formation conforms with the Pabdeh Formation, while the upper boundary conforms with the Gachsaran Formation. Based on the lithological characteristics observed, the Asmari Formation has a thickness of approximately 400 m and is subdivided into five zones: As-1, As-2, As-3, As-4, and As-5.

The Miocene Gachsaran Formation forms an effective cap rock above the Asmari reservoir (Motiei, 1995). The quality and sedimentary characteristics of the Asmari Carbonate Formation in the Qaleh Nar Oilfield vary significantly both vertically and horizontally, even over short distances. As a result, this reservoir is complex and heterogeneous, posing challenges for petroleum geologists and reservoir engineers in the development of oilfields and the planning of enhanced oil recovery programs. In many hydrocarbon fields within the Dezful Embayment, including the Qaleh-Nar Oilfield, it is not feasible to assume a uniform reservoir quality for a specific layer or reservoir zone within the Asmari Formation (Jamilpour et al., 2024).

3. Data and processing methods

A cross-dipole log is acquired using the Schlumberger DSI tool. The tool is a multi-receiver tool with a linear array of eight receiver stations, one monopole transmitter and two orthogonal dipole transmitters. At each receiver station, a pair of orthogonal dipole receivers that form two arrays are located. Each of these is oriented in the direction of the dipole transmitters. Data acquisition is performed in the same reference line of the transmitter (inline) and at 90° angles (cross-line). Waveform data at each depth for anisotropy analysis are collected as four components: the output of the dipole receivers aligned (inline) and orthogonal (crossline) to each dipole transmitter (Esmersoy et al., 1994). The combination of those sources and receivers enables us to record the full waveform of all types azimuthally. Dipole sonic logging enables measurement of the fast and slow shear wave velocities caused by shear splitting and radial variation of shear speed into the formation (Burridge and Sinha, 1996; Esmersoy et al., 1994, 1995). Since both shear dipole and Stoneley wave measurements are available, an accurate evaluation of a transversely isotropic medium can be accomplished (Pistre et al., 2005).

The workflow in this study as depicted in Fig. 2 includes analysis of an Ultrasonic Sonic Imager (UBI/OBMI) and Dipole Sonic log, which consists of Shear Anisotropy, Flexural Dispersion Analysis and Stoneley Reflection Analysis. As shown in the following diagram the suggested workflow for anisotropy analysis and dispersion analysis consists of five major parts:

The workflow starts with the preparation of acquired sonic data for all subsequent processing.

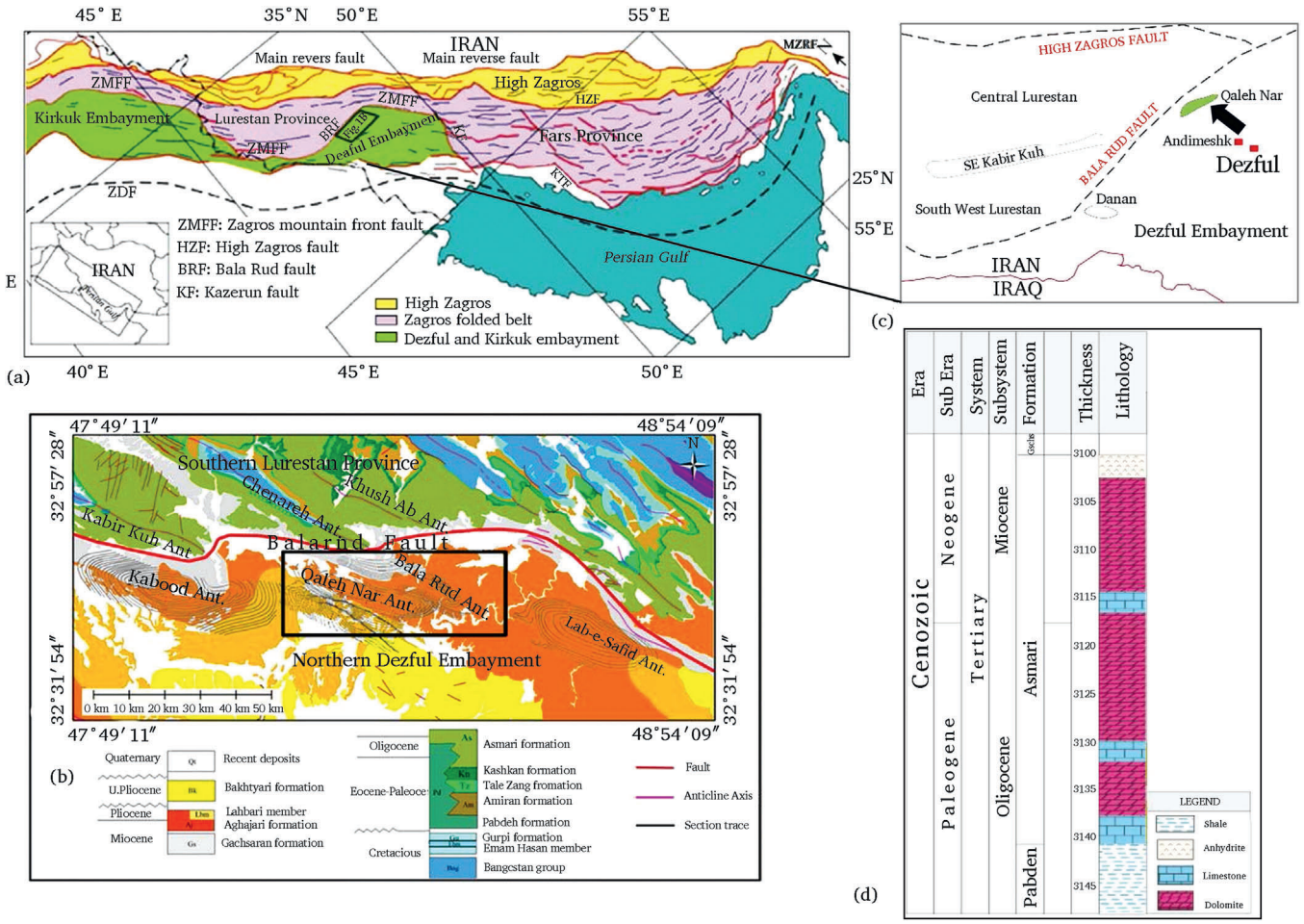

Fig. 1. (a) Location of the studied area in the central Zagros, (b) simplified geological map of the study area and location of the subsurface anticlines concerningBalarud fault (Razavi Pash, 2020), (c) Location of Qaleh-Nar Oilfield in Dezful Embayment and (d) Lithostratigraphy of the Asmari Formation in the Qaleh-Nar Field.

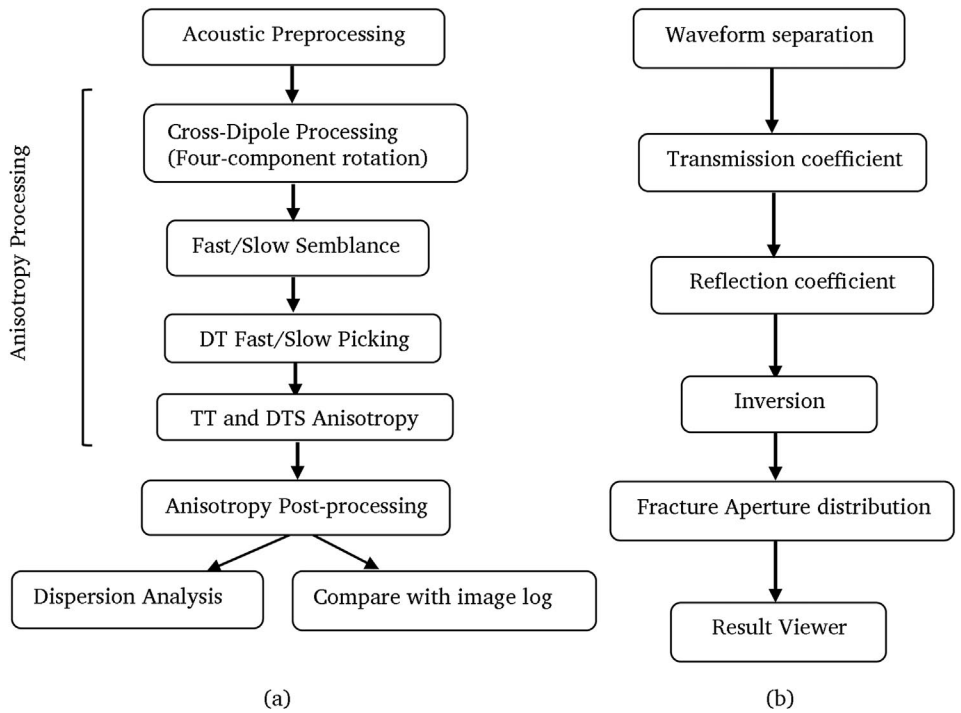

Fig. 2. (a) Anisotropy processing workflow and (b) Stoneley fracture analysis.

3.1. Acoustic preprocessing

This step ensures that all tool-specific preprocessing is conducted and that the depth reference for DSI tool is honored before starting the quality control of the data. This preprocessing module performs the following operations:

1 Cross-Dipole waveform data for anisotropy is collected as four components: the output of the dipole receivers aligned (inline) and orthogonal (crossline) to each dipole transmitter [XX, XY, YX and YY]. Normalization logs are based on the gain variable created by the Data Preparation module.
2 In anisotropy preprocessing, one tool azimuth input (RB, P1AZ) is mandatory.
3 Shear slowness (DTS) and travel time (TTS) logs and Caliper.

Waveforms are typically referenced from a single point in the tool. Different tools may use various reference points, such as the middle of the receiver array (R-R), the midpoint of the transmitter-to-receiver spacing (T-R), or the bottom of the tool. For DSI, the reference point is at the bottom of the tool.

3.1.1. Quality control

Delta-T or Slowness (DT) Results. Delta-T Compressional (DTCO) was computed from both MF (Monopole Far) receiver and transmitter mode. Far Monopole shows good quality waveforms giving reliable compressional slowness over open-hole section except few intervals where data quality is affected by rugose hole (Fig. 3).

DTSM (Delta-T shear) was computed from both X-dipole, Y-dipole and Monopole and the processed DTSM was reliable over most of the interval. Y-Dipole has higher coherence compared to X-Dipole mode, so the final shear slowness (DTSM) was computed from Y-Dipole mode.

Delta-T Stoneley (DTST) was extracted from Monopole low frequency (MF_ MST). High-quality DTCO, DTSM and DTST were extracted over the entire interval. Figure 3 displayed a composite plot of extracted slowness, Semblance of Monopole, XX Dipole, YY Dipole and Stoneley, PR and VP/VS ratio.

Vp/VS Plot: The Vp/Vs plot displays the recomputed DT-compressional and DT-shear values. This plot shows the type of dominant lithologies present are limestone and dolomite, which characterize an acoustically fast formation (Fig. 4). The quality of the cross-dipole measurements was generally good allowing for confident interpretation of the results.

Generally speaking, the quality control (QC) of log data is the fundamental starting point for obtaining reliable curves and, facilitating accurate interpretation. The acoustic measurements are even more important since the sonic log is the result of a complex processing of a huge amount of raw data: the tool is multi-samples, and multi-sensors and it can acquire several sets of waveforms for a single depth. Therefore, the cross plot of VP/VS versus DTCO helps us quality control the results and identify the formation type (Fast, Intermediate or slow) selection which is important during semblance processing.

3.2. Four-component rotation

This module calculates shear wave anisotropy directions and variations in relative magnitude from cross-dipole measurements. The Four-component rotation is the first step of the Anisotropy processing workflow. This module applies the Alford (1986) rotation technique to compute the slow and fast shear waves and their directions in an anisotropic formation with a vertical transverse isotropy. The resulting waveforms corresponding to the fast- and slow-shear shear orientations are then subjected to semblance processing to obtain the fast- and slow-shear slowness (Esmersoy et al., 1995; Kimball and Marzetta, 1986).

Alford rotation, align waveforms, and calculation and evaluation of derived fast and slow components are done for deriving the azimuth of the fast shear wave for each bandwidth of waveforms (Alford, 1986). The dominant trend of the azimuth of anisotropy is aligned with the azimuth of the fast shear wave. The Fast shear azimuth (FSA) obtained is equal to the sum of the tool azimuth and the rotation angle applied to the waveforms to eliminate the crossline energy as shown in the equation:

$$\mathrm{FSA} = \mathrm{ToolAzimuth} + \mathrm{WaveRotationAngle}$$

3.3. Fast/slow shear semblance analysis

This module processes the fast and slow shear waves to output semblance (STC) and projection logs. Semblance processing looks for similarities in waveforms across the receiver array. This is done by correlating the waveforms within a user-defined time window over a range of angles, that is, slowness. Setting limits to specify processing time range will increase processing speed and may improve processing quality by eliminating unwanted early and late arrivals from the semblance process. To remove unwanted frequency components, frequency filtering is applied using a bandpass filter set between 1 and 3 kHz. In the low bandwidth frequency (1–3 kHz), the differences in slowness, energy, travel time, and penetration depth are more extreme than those recorded by the other bandwidths considered. The semblance spectrum shows the distribution of coherence values across the frequency axis. When the waveform signals are best correlated, the coherence is at its maximum.

The picking module tracks the coherence maxima on the projection log to create continuous slowness logs. The picking can be done using either a seed value or a guide log.

3.4. Anisotropy post-processing (TT, DTS anisotropy)

Anisotropy post-processing is the final part of the Anisotropy processing workflow. This method calculates slowness and time-based anisotropy along with final Fast shear direction based on the use of gamma-ray, hole size, and time-based anisotropy. It also outputs smoothed versions of the fast and slow shear slowness.

$$\text{Slowness} - \text{based Anisotropy} : \mathrm{SLOANI} = \frac{\mathrm{DTSM_{Slow}} - \mathrm{DTSM_{Fast}}}{(\mathrm{DTSM_{Slow}} + \mathrm{DTSM_{Fast}})/2} \times 100$$

$$\text{Time} - \text{based anisotropy} : \mathrm{TIMANI} = \frac{\mathrm{TDIF}}{\mathrm{TTFAST}} \times 100$$

where, TDIF: Arrival time difference between fast and slow shear waves and TT Fast: Fast shear arrival time

Cross energy difference: XENEDIF = MAXE-MINE

After running the Cross-Dipole Processing and TT & DTS Anisotropy modules, anisotropic zones can be identified by following these criteria:

- There should be a significant difference between the minimum and maximum cross-line energy.
- The fast azimuth should remain relatively stable.
- If the tool is rotating, the fast azimuth should not mimic the tool's rotation.
- Anisotropic zones will exhibit a noticeable time delay between the first shear arrivals of the slow and fast principal waveforms, leading to relatively high TT & DTS anisotropy values.
- The borehole radius should be consistent. Irregular hole conditions, such as washouts, can create delays between the two principal waves, which may incorrectly suggest anisotropy (Zakharova and Goldberg, 2015).

3.5. Dispersion analysis

Dispersion analysis of dipole flexural wave provides critical

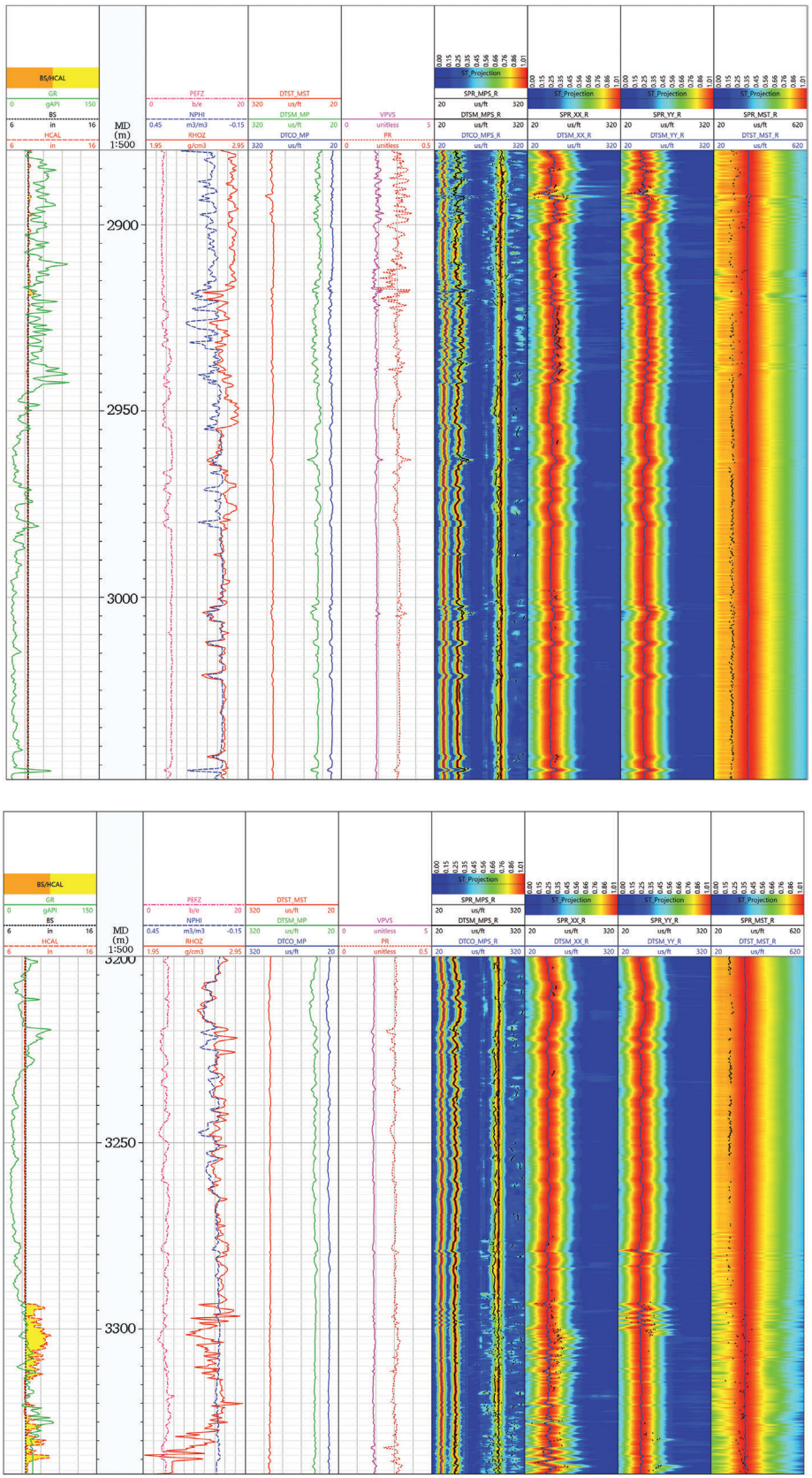

Fig. 3. Composite plot of extracted slowness along with continuous Semblance map of Monopole, Dipole (XX and YY), Stoneley, PR and VPVS. Track 1: GR and Caliper; track 2: Depth; track 3: Neutron-Density log and PEF; track 4: Compressional Slowness (DTCO), Shear slowness from Monopole (DTSM); Stoneley Slowness (DTST); track 5: Poisson ratio (PR) and VP/VS; track 6: Semblance map of Monopole; Track 7: Semblance map of XX Dipole; track 8: Semblance map of YY Dipole. Track 9: Semblance map of Stoneley.

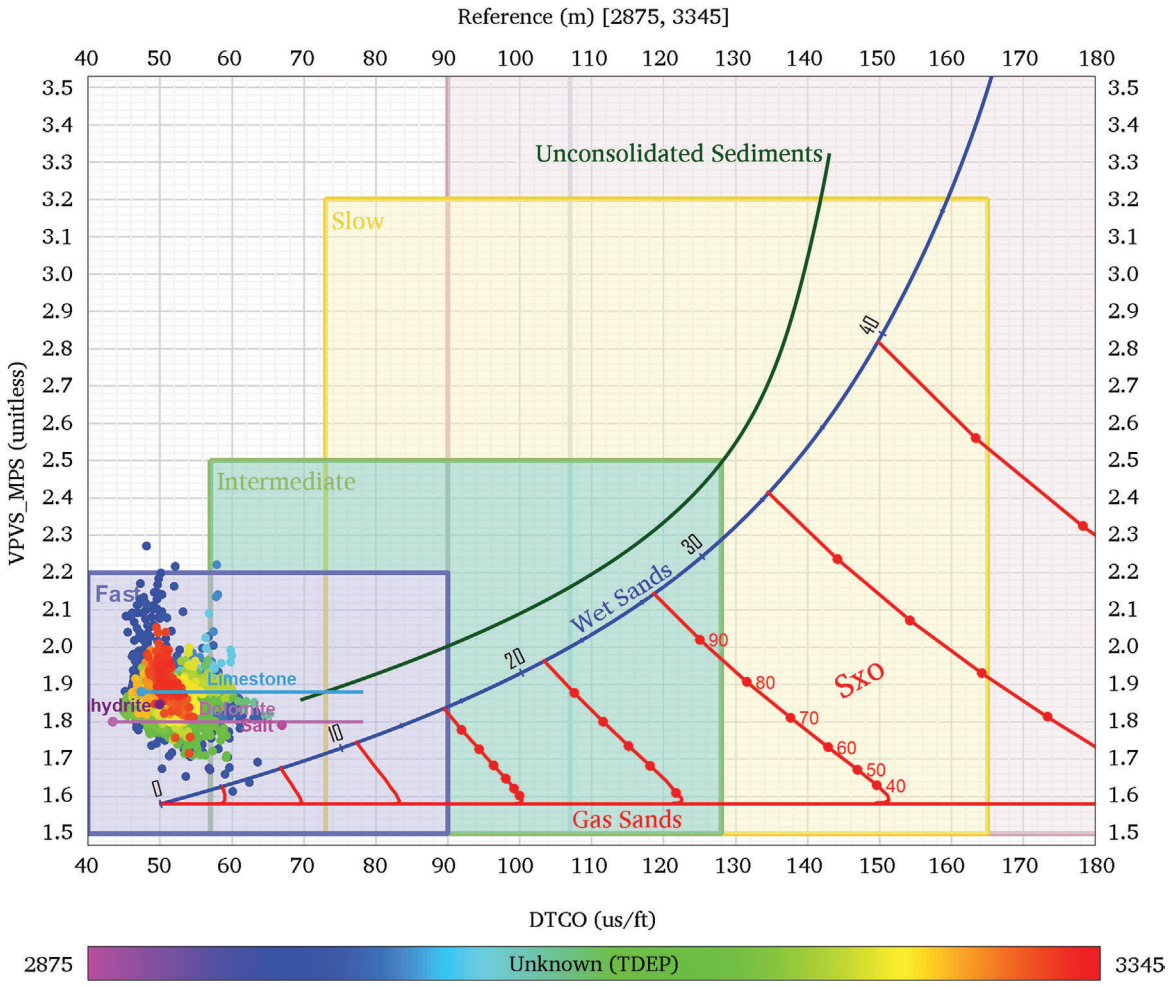

Fig. 4. Cross-plot of VP/VS ratio and DTCO used to identify different lithology and Formation type as well as the fluid type.

constraints to decipher the nature of anisotropy present in the formation (Franco et al., 2006; Plona et al., 2002). Dispersion plots are graphical representations of frequency versus slowness for the different wave types. Analysis of the shear slowness variations in the frequency domain and the inversion of discrete slowness over a wide frequency band allows us to obtain the shear radial profile, therefore, the dispersion plot enables us to determine whether the formation is isotropic or anisotropic, homogenous or heterogeneous (Burridge and Sinha, 1996).

3.6. *Compare fast shear azimuth with image log*

The azimuth of the fast shear wave as the azimuth of anisotropy and its corresponding intervals are then compared with the results of the image log for the same interval. This made it possible to reject or confirm the findings of the DSI acoustic anisotropy analysis for each bandwidth considered.

Ultrasonic Borehole Image Log (UBI) was processed to generate amplitude and travel time images, which were used to identify and characterize the natural fractures and differentiate them from drilling-induced wellbore failure. Stress-induced wellbore breakouts are visible in acoustic amplitude and travel time images due to the large contrast in acoustic impedance between a fluid-filled fracture and the matrix. The difference in fast and slow shear wave velocities and the azimuth of the fast shear from anisotropy analysis indicate the maximum horizontal stress azimuth as well as provide the key inputs to characterize the minimum horizontal stress. Integrating this result with the breakout analysis from the acoustic borehole images provides the comprehensive state of the in-situ stresses (Das et al., 2021).

3.7. *Fracture detection using stoneley wave*

When low-frequency Stoneley waves encounter open permeable fractures at the borehole wall, some of the wave energy is reflected while some are lost in the fracture (Bakku et al., 2012). Therefore, the two primary effects of open fractures on acoustic waves are:

i. Reflections of Stoneley waves causing Chevron patterns.
ii. Reduction in wave amplitude (attenuation).

The workflow shown in Fig. 2 illustrates the fracture analysis using the Stoneley waveform.

3.7.1. *Waveform separation*

In the presence of open fractures intersecting the borehole, the Stoneley wave will attenuate and also generate a reflected wave from the discontinuity between the fracture and borehole wall. This module separates Stoneley waves into direct, down-going and up-going reflected waves. Required inputs for the calculations are the low-frequency Stoneley waveform data and the Stoneley slowness log. Then, the Stoneley wave reflection coefficient is obtained.

3.7.2. *Reflection/transmission coefficient*

Once the frequency range (min/max limit) for reflection and transmission coefficient is determined using dispersion plot, then, the result of waveform separation is used for reflection and transmission coefficient processing, and both sets of the results are used as input for a combined fracture aperture inversion (Brie et al., 1998b). The reflection

coefficients can be used as an indicator for the presence of permeable fractures in the borehole.

3.7.3. Fracture aperture distribution

The inputs for fracture aperture distribution are computed in fracture analysis which include transmission and upgoing/down-going reflection coefficients. Once it is finished, the inversion process can be executed. The larger the fracture width, the larger the reflection coefficient will be. This type of analysis is useful for wells where borehole images have not been acquired.

4. Interpretation of field data

4.1. Ultrasonic borehole imaging (UBI) result

The UBI utilizes a high-resolution transducer to create acoustic images of the borehole wall. This transducer emits ultrasonic pulses at a frequency of 400 kHz. These pulses are reflected off the borehole wall

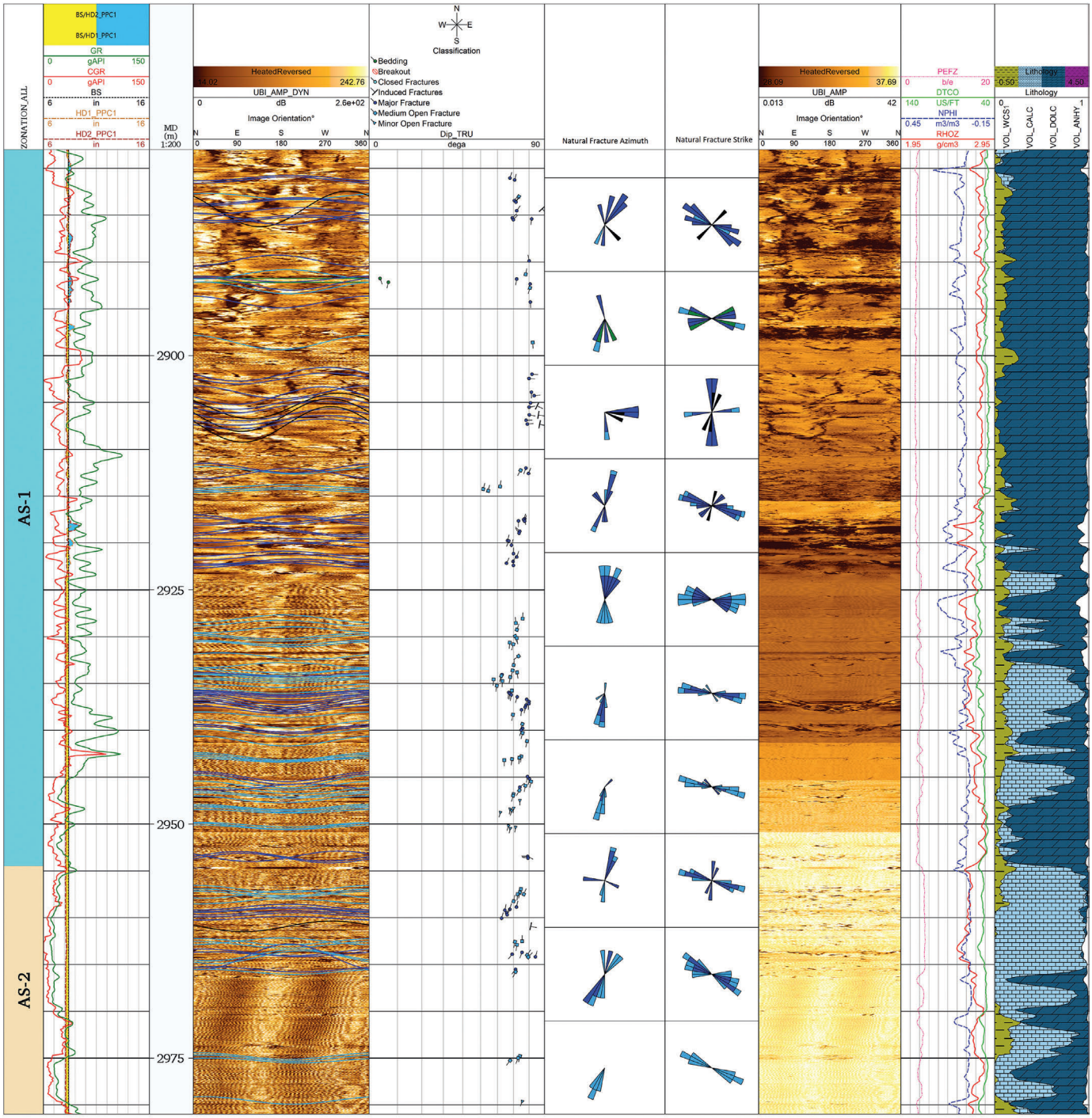

Fig. 5. Integrated display of UBI Image, Gamma ray, porosity and lithology of Asmari reservoir. Track 1: GR, bit size and caliper; Track 2: Depth; Track 3: UBI Dynamic Image displaying fracture traces; Track 4: Fracture's Dip; Track 5: Fracture's Azimuth; Track 6: Fracture Strike; UBI Static image; Track 7: Fullset porosity curves and PEF; Track 8: Lithology. UBI Image shows Major open fractures, medium open fractures plus minor indication of drilling induced fracture. The Image indicates that the orientation of the fractures has changed above 2925 m.

and received by the same transducer. The system measures both the amplitude and travel time of the reflected signals. By continuously rotating the transducer and moving the tool upward, a complete map of the borehole wall is generated.

Based on the results from the borehole imaging, we identified various fractures throughout the entire logged interval of the study well. These fractures were classified as major, medium, and minor open fractures, as well as closed fractures along the bedding plane. Additionally, we noted induced fractures and breakouts. Major natural fractures are the most easily detected on the borehole images. They are characterized by a continuous sinusoid-formed trace on the images. Drilling-enhanced natural fractures can look similar to drilling-induced tensile fractures on borehole images. However, we can distinguish between them using several criteria. The natural fractures exhibit a flexible sinusoidal fit on the feature; this is because natural fractures are usually planar features, discordant to bedding. In vertical wells, dipping fractures appear as sinusoidal traces, while vertical fractures show up as straight lines. In deviated and horizontal wells, naturally occurring fractures also display sinusoidal traces, and the flexible sinusoid will align perfectly with the fracture trace (Mahmood and MacPherson, 2014).

On the other hand, drilling-induced fractures can be identified in vertical wells because they form pairs of symmetrical fracture tracks that run parallel to the borehole (180° apart), and are oriented parallel to the principal stress direction. These fractures develop asymmetrically within the wellbore and are typically non-planar, making it difficult for them to fit a sinusoidal pattern. By carefully applying these basic criteria, we can effectively distinguish between natural and drilling-induced fractures (Mahmood and MacPherson, 2014).

The analysis of the acoustic image log also revealed multiple preferential directions of fractures, primarily oriented towards the SSW, NNE, NE, and East, with corresponding strike directions of WNW-ESE, NW-SE, and N-S (Fig. 5). By comparing the acoustic images with the dispersion analysis from the anisotropy processing, we can determine which of these identified fractures are propagating away from the borehole wall.

4.2. Anisotropy analysis

In a vertical well of approximately 8.375 inches in diameter, located in the Qaleh-Nar Oilfield in Southwest Iran, a full-waveform sonic log

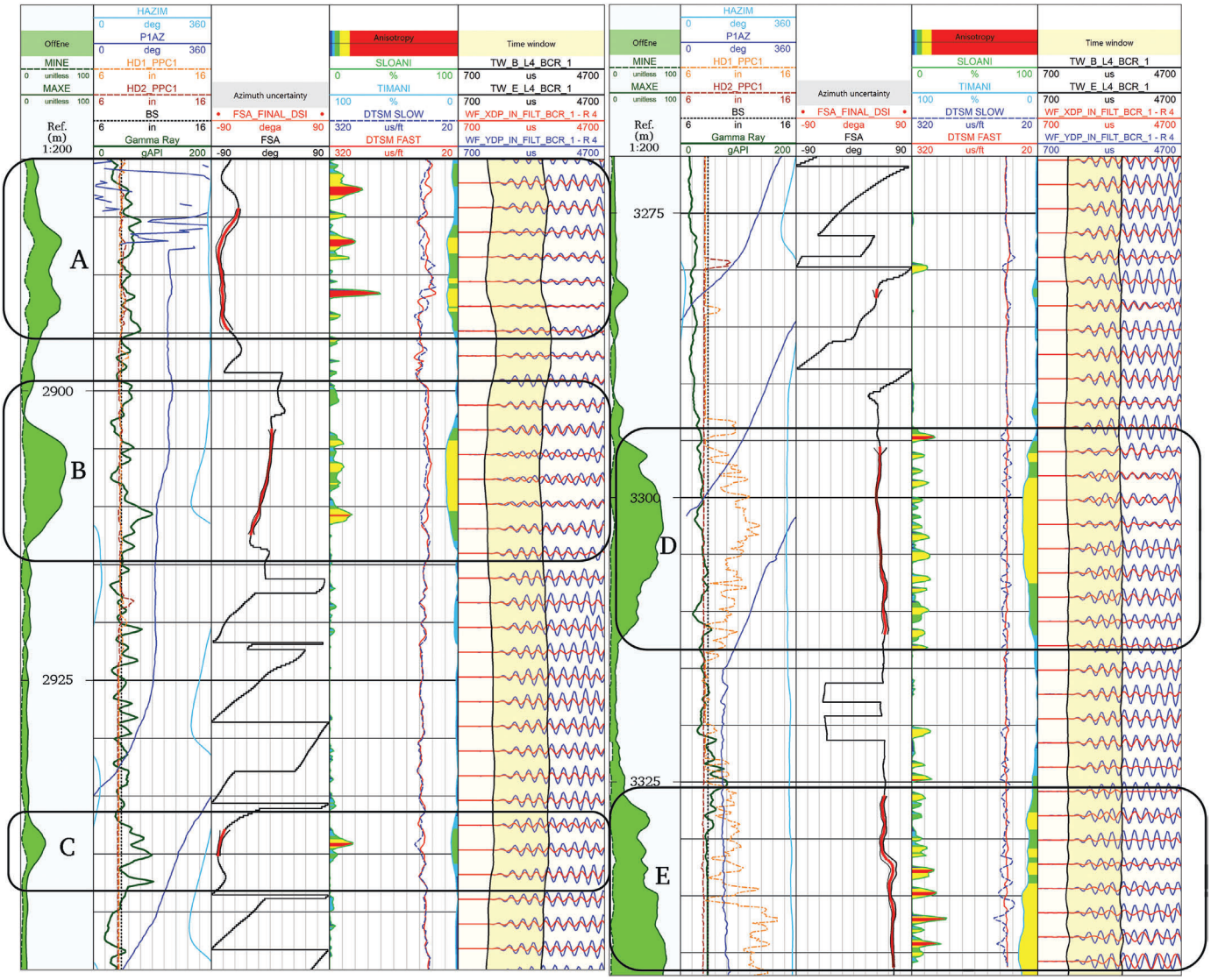

Fig. 6. Cross-dipole anisotropy processing of flexural-wave data to determine fast and slow shear slowness, along with polarization direction of the fast shear wave. The depth track shows the differences in the minimum and maximum cross-line energy from the fast and slow dipoles. Track 2: Tool and hole orientation (P1AZ and HAZIM), GR, Bit size and Dual-Caliper. Track3: Fast shear azimuth direction (red). Track 4: Slowness anisotropy (DT-based), time-based anisotropy and fast and slow shear slowness. Track 5: the processed waveforms at level 4 of the fast and slow dipole firing.

(DSI) was acquired. This log was utilized to obtain waveforms for compressional monopole, cross-dipole, and Stoneley waves. The dipole waveforms were processed to determine the slowness of both the fast and slow shear waves, as well as the polarization azimuth of the far-field fast shear wave (Donald et al., 2013; Esmersoy et al., 1994). The results of this analysis, which include the anisotropy findings and the STC projections of the rotated flexural data, are illustrated in Fig. 6. The plot reveals five main zones that exhibit significant shear-wave splitting.

This study presents three different methods for calculating shear-wave anisotropy, focusing on the time, slowness, and energy of the dipole shear waveform. First, we analyzed shear-wave energy anisotropy, which is determined by the minimum and maximum differences in cross-component energy. This discrepancy is the most straightforward indicator of anisotropy (Fig. 6, track 1). Large energy differences, particularly when the minimum energy remains low, suggest significant shear-wave splitting and highlight areas of interest. In particular, five intervals-2880–2895 m, 2902–2912 m, 2937–2940 m, 3293–3313 m, and 3325–3340 m—exhibit significant anisotropy (Fig. 6).

Second, travel time anisotropy-reflected in the significant shear-wave travel time indications based on the arrival times of the fast and slow waves correlates well with the energy anisotropy indications throughout the interval (Fig. 6, track 6).

The third measurement of anisotropy, slowness anisotropy, is derived from the computed slowness of the shear-wave fast and slow components using slowness-time coherence (STC) processing (Fig. 6, track 6). This measurement serves as the primary indicator of the magnitude of shear wave anisotropy. The detailed analysis of shear waves suggests that the anisotropic properties originate from within the reservoir and are not influenced by near-wellbore stress concentrations.

The anisotropy is identified using several key factors: a strong signal, the difference between the maximum and minimum energy in Alford rotation, the arrival time difference, a stable fast-shear azimuth, a small uncertainty in the azimuth, and the distinction between slowness and the clear separation of dispersion curves for fast and slow-shear directions. In the interval of 2880–3340 m, we selected five zones for interpretation: A (2880–2895 m), B (2902–2912 m), C (2937–2940 m), D (3293–3312 m), and E (3326–3340 m).

Shear dispersion analysis is used to identify the source of acoustic anisotropy. This is essential because not all observed wave splitting results from stress alone; recognizing the true drivers behind these phenomena enhances our overall comprehension and ability to address the underlying factors effectively.

4.3. Dispersion analysis

This study utilized flexural-wave anisotropy analysis to investigate the characteristics of fast and slow shear waves and classify the formation anisotropy. Fig. 7 presents the results, which include the SFA and STC projections of the rotated flexural waveform. Five main zones exhibit significant shear-wave splitting, highlighted by the green shaded band in the depth track representing maximum-minimum cross-line energy. The computed percentage of slowness anisotropy exceeds 16% in certain intervals, as denoted by the red shading along the left edge of the DT-based anisotropy curve (Fig. 7). Additionally, it is important to note that the polarization of the fast shear wave, or fast shear azimuth, is not constant throughout the interval and remains independent of tool rotation.

At discrete depths, the fast (red) and slow (blue) flexural waves were transformed to the frequency-slowness domain to generate slowness-dispersion curves. Dispersion analysis is a crucial tool for confirming that the observed anisotropy is a direct result of stress imbalance. It not only validates the slowness of anisotropy but also helps identify the dominant mechanism of anisotropy. Shear anisotropy can arise from various factors, including layering, fractures, and stress imbalance. The following section will discuss how dispersion curve analysis can be used to identify the source of anisotropy.

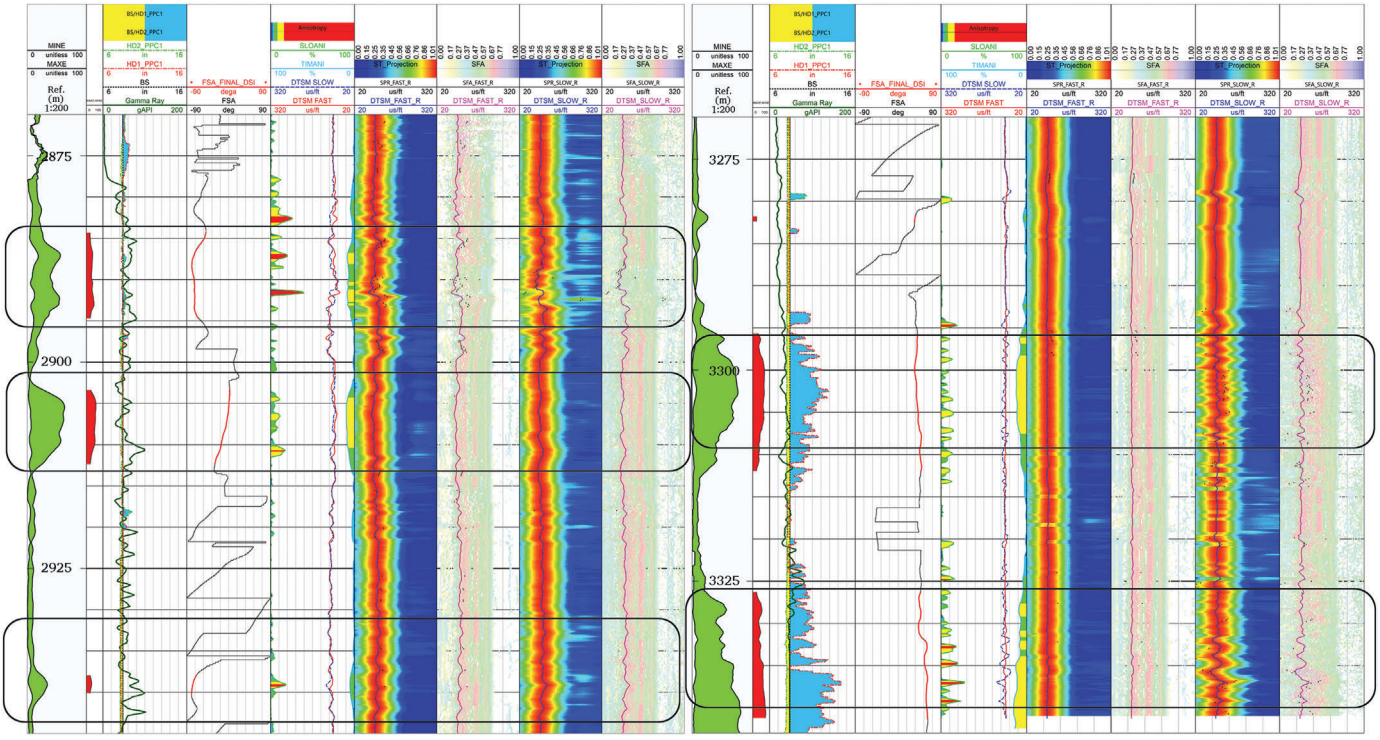

Fig. 7. Borehole anisotropy analysis including the SFA and STC projections for the fast in-line and slow cross-line waveforms (track 6,7 and track 8,9). Five main zones exhibit significant shear-wave splitting as shown with a green-shaded band in depth track and red-shaded in track 2 (max-min cross-line energy). Track 3, caliper, bit size, GR; Track 4, Fast Shear Azimuth (FSA). This analysis is also represented with colour-shaded band in DT-based anisotropy (SLOANI) and time-based anisotropy (TIMEANI) in Track 5.

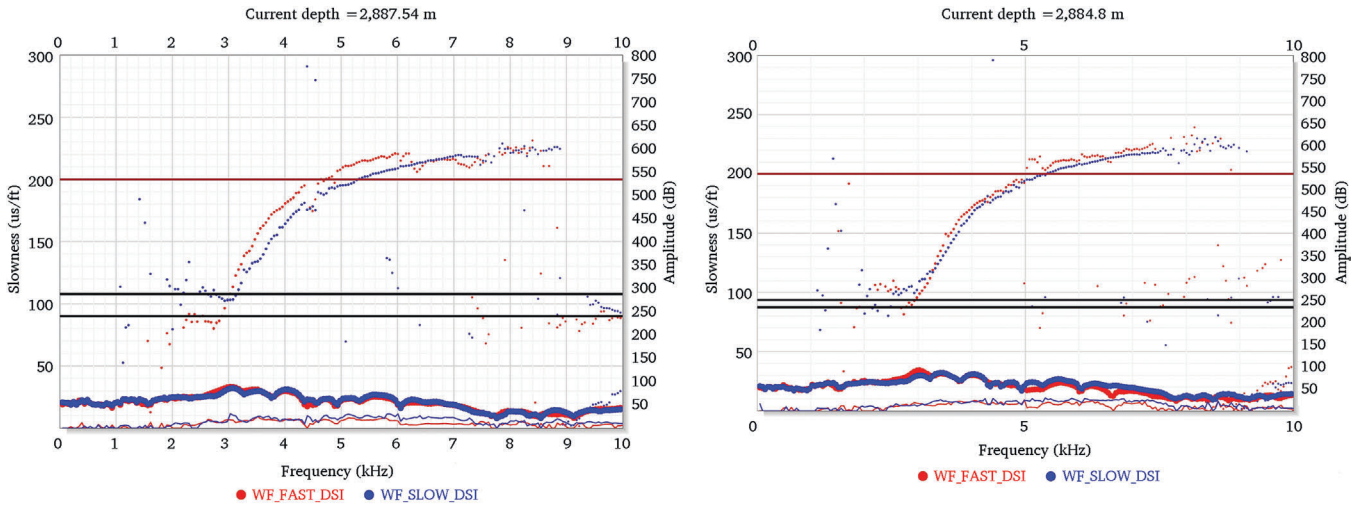

Fig. 8. Dispersion plot for depth 2884.8 m (left) and depth 2887.54 m (right). Fast dipole dispersion (red), slow dipole dispersion (blue) The crossing-over dispersion profile for the fast and slow shear indicates stress-induced anisotropy.

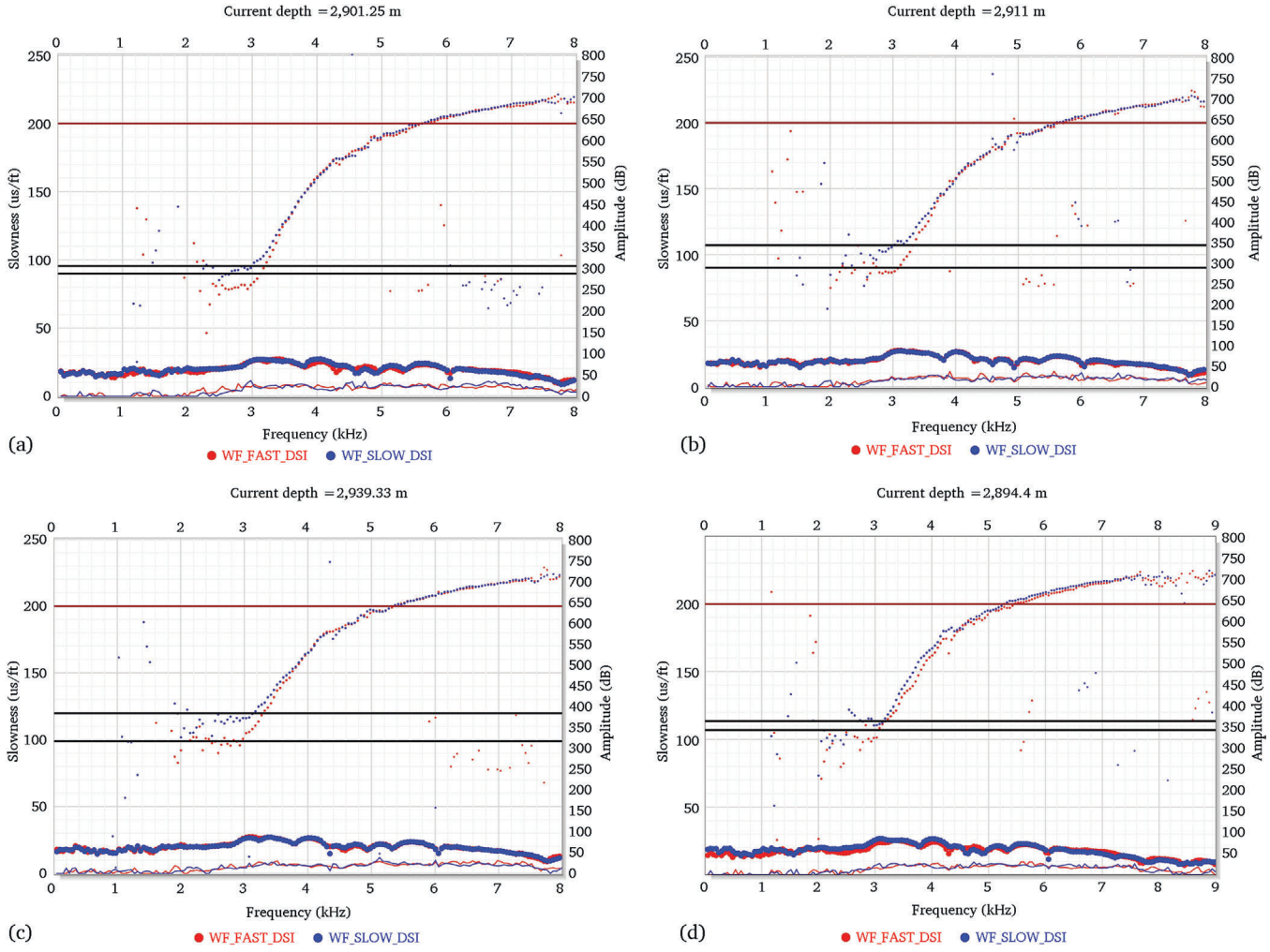

Fig. 9. Parallel dispersion curves from a naturally fractured formation. Fast dipole dispersion (red), slow dipole dispersion (blue). [Dispersion plot for depth 2901.25 m, 2911 m, 2939.33 m and 2894.4 m within the fractured zone].

4.3.1. Identify stress-induced anisotropy

It is well known that stress-induced anisotropy results in azimuthal variation in shear-wave slowness, as well as differences in shear-wave slowness between far-field and near-field measurements caused by hoop stress around the borehole (Sinha and Kostek, 1996). Fig. 6 shows the results of anisotropy processing from the dipole shear sonic log over the logged interval of a carbonate sequence, specifically the Asmari Formation and the top of the Pabdeh Formation. Throughout most of the

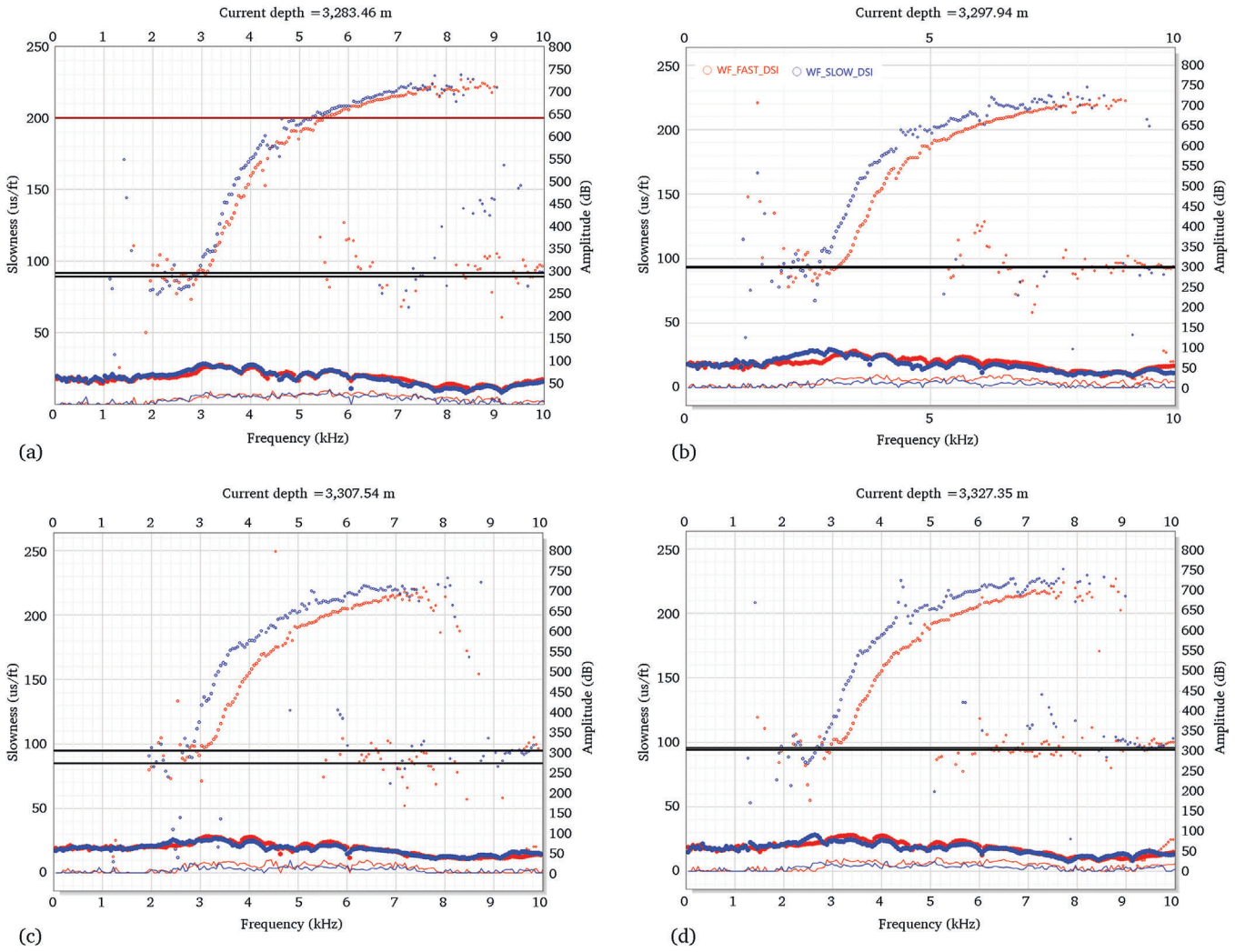

Fig. 10. Dispersion plots for depths 3283.46 m, 3297.94 m, 3307.54 m, and 3327.35 m, indicate mechanically damaged formation; Fast Shear (red) and slow shear (blue).

logged interval, which features a limestone/dolomite sequence, the dual calipers remain within the 10% ovality criteria. However, in the bottom interval from 3293 to 3340 m, breakouts are observed on both the caliper and the ultrasonic image log (Fig. 7). In the bottom interval, some depths exhibit ovality of less than 10%, which have been selected for dispersion analysis. The anisotropy plot indicates that shear wave anisotropy exceeds 10% in nearly all five zones (Fig. 7). Fig. 8 illustrates the dipole dispersion crossover of fast (red) and slow (blue) flexural waves at specific depths. The data indicate anisotropy, and we note a dispersion-curve crossover at about 3.2 kHz. This crossover, observed in the dispersion analysis, suggests that drilling-induced fractures are present at this interval (Cheng, 2015; Donald et al., 2013).

Table 1
Fast Shear Azimuth and dominant anisotropy mechanism.

Formation	No	Interval (m)	Fast shear Azimuth (Anisotropy Strike)	Dominant Mechanism
As-1	1	2880–2895	NW-SE to E-W (WNW-ESE)	Natural Fracture
As-1	2	2902–2912	N-S to NNW-SSE	Natural Fracture
As-1	3	2937–2940	WNW-ESE	Natural Fracture
As-5	4	3293–3312	NE-SW	Breakouts
Pabdeh	5	3326–3340	NE-SW	Breakouts

4.3.2. *Identifying intrinsic anisotropy*

Another key mechanism of elastic anisotropy can be identified through dipole sonic measurements that are not influenced by differential present-day stress. Open fractures can also lead to dipole shear anisotropy (Donald et al., 2015; Prioul et al., 2007). In this case, dipole dispersion analysis reveals that, at low frequencies, the fast and slow shear modes are parallel to each other, with the slow shear slowness being greater than that of the fast shear. However, at higher frequencies, these modes overlap (Fig. 9).

The dispersion analysis conducted on the fracture interval confirms the presence of propped fracture anisotropy. Examples of this analysis are shown in Fig. 9. The dispersion plots at varying depths within the fracture zone reveal a consistent propped fracture signature, indicated by parallel dispersion curves. Additionally, the velocity differences between fast and slow shear waves are greater at lower frequencies.

4.3.3. *Identify borehole ovality*

The near-wellbore region is significantly affected by the drilling process and the resulting concentration of stress in the borehole, which leads to variations in shear slowness (Plona et al., 2002). While borehole ovality can arise from differential horizontal stresses, it is crucial to accurately identify and exclude highly enlarged areas when conducting dispersion analysis and assessing sonic anisotropy. Additionally, borehole ovality can impact the calculation of slowness anisotropy if the

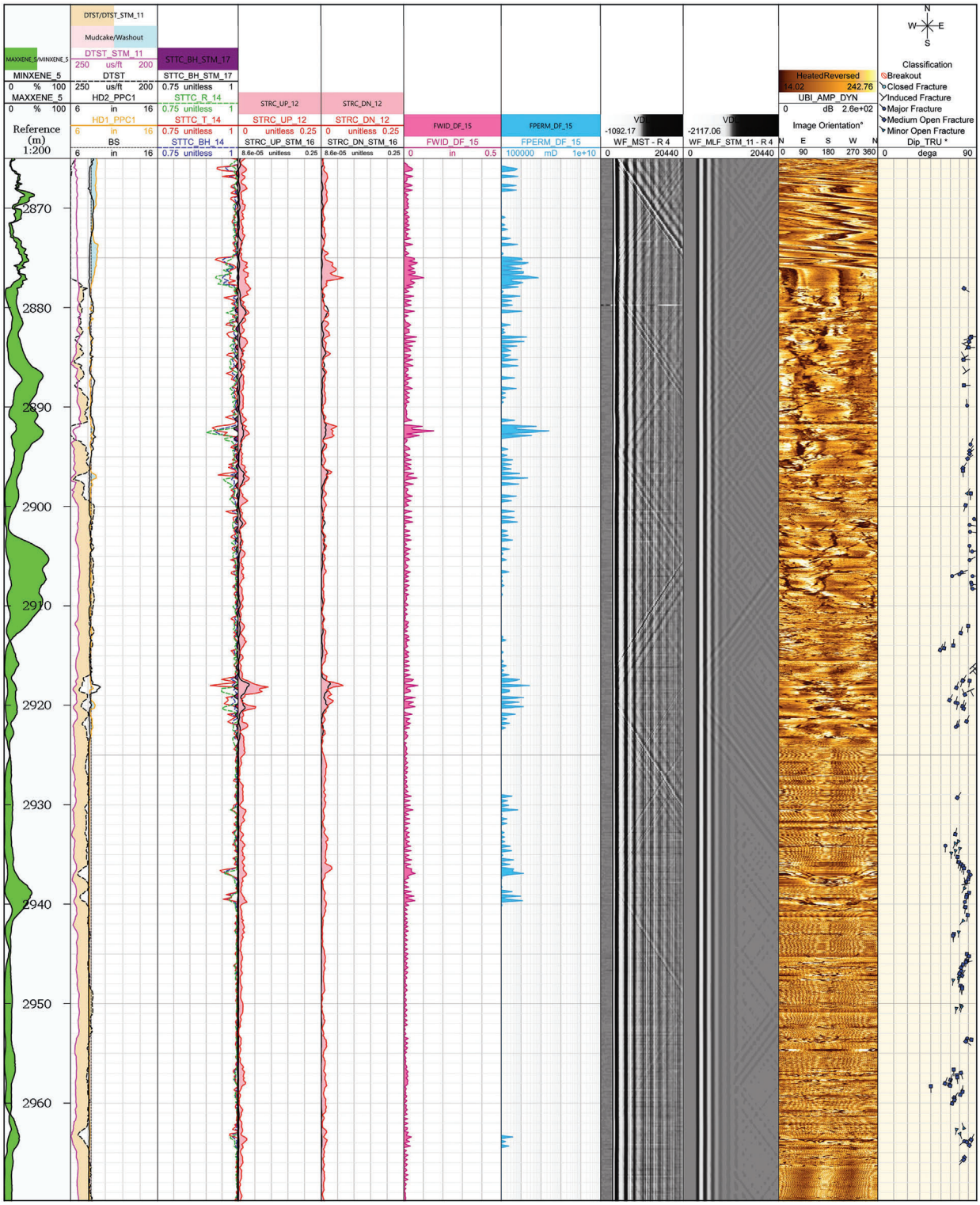

Fig. 11. Stoneley reflection and attenuation analysis and Ultrasonic Image data, comparing fracture detection from Stoneley and UBI image. In the depth track, minimum and maximum cross-line energy differences from the shear wave anisotropy analysis. Track 1, Caliper, Bit size, measured DT Stoneley (DTST) and modelled elastic DT-Stoneley (DTST-STM) with the difference shaded in orange; Track 2, Stoneley transmission coefficients from the transmitter (TRA), receiver (REC), borehole compensated (BHC) and Tezuka borehole compensated modelled (BH_STM) arrays. Track 3 and 4, reflection coefficients for the up-going and down-going measured and modelled Stoneley waveforms, respectively. Track 5, Stoneley fracture aperture from the inversion of the transmission and reflection coefficients. Track 6: Stoneley fracture permeability computed from the aperture in Track 5; Track 7 and Track 8, Level 4 Stoneley waveforms for the measured and Tezuka model data; Track 9: Ultrasonic image with true birth corresponding to 0°. Track 10: fractures dip and azimuth.

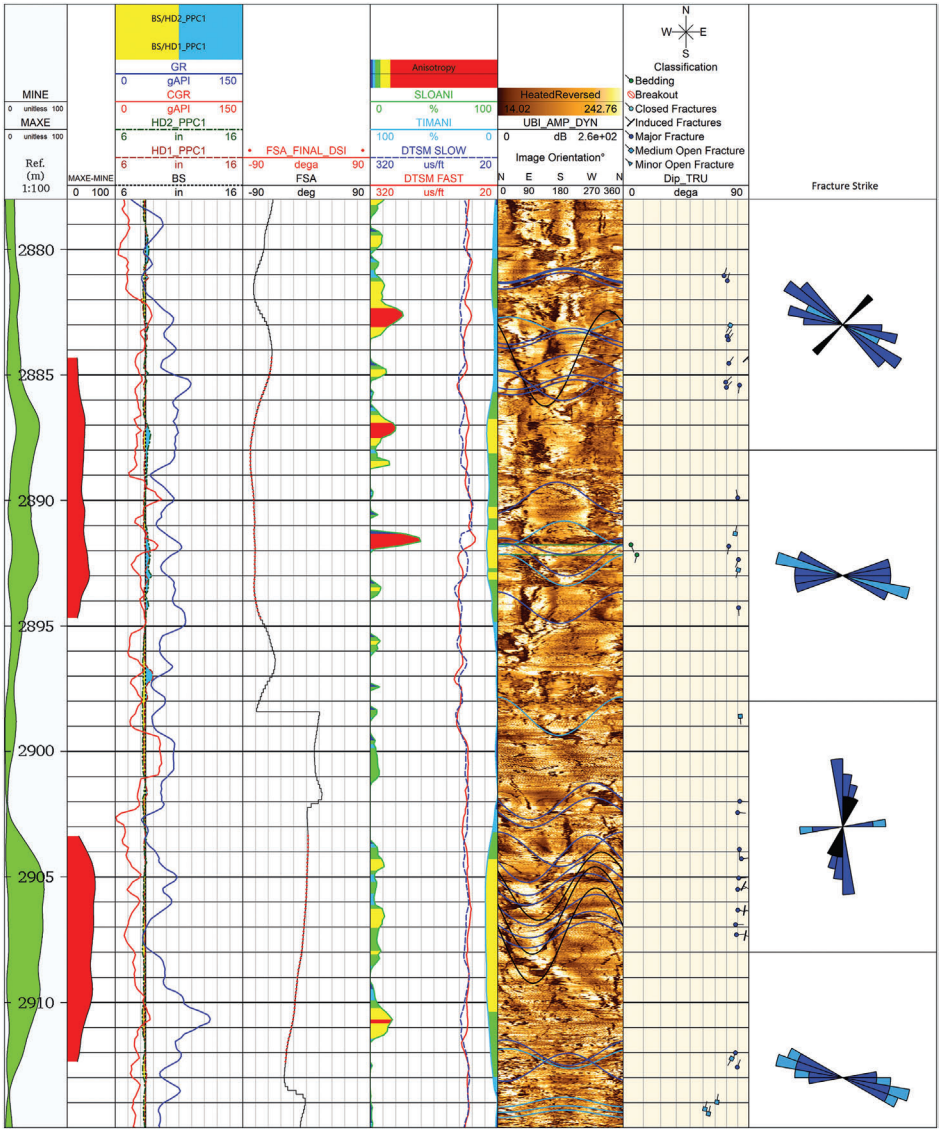

Fig. 12. Dipole sonic anisotropy with the associated acoustic borehole image [2880–2915 m].

frequency filtering or waveform processing during sonic pre-processing is not optimal (Donald et al., 2015). This ovality may also hinder the accurate identification of the crossover point and the anisotropy mechanism. Therefore, for dispersion analysis, we only consider intervals with an ovality of less than 10%.

In this well, breakouts are detected at two intervals at the bottom, based on data from both the dual-calipers of the DSI log and the Ultrasonic Image Log. Breakouts serve as reliable indicators of stress directions. Dispersion analysis conducted at various depths within the bottom interval, specifically from 3280 to 3313 m and from 3325 to 3340 m, reveals that the dipole dispersions are offset at the middle and higher frequencies (Fig. 10). This pattern suggests that breakouts are present within this interval.

Dispersion curve analysis confirms the slowness anisotropy and helps us identify the dominant anisotropy mechanism. Table 1 shows the primary source of anisotropy at various intervals of the study well.

4.4. *Stoneley wave analysis*

The Stoneley wave is a guided mode that travels along the borehole wall in a piston-like motion, acting as a pulse that radially contracts and expands the borehole equally in all directions (Donald and Bratton, 2006). This wave has been studied as a method for detecting and evaluating fractures (Hornby et al., 1998; Zaree et al., 2016). In intervals where fractures exist, particularly in permeable formations, the energy of the Stoneley wave significantly attenuates (Xiang et al., 2015). The borehole fluid that fills these fractures can reduce the velocity of the Stoneley wave, leading to dispersion and further attenuation (Almalki et al., 2013). Attenuation of direct Stoneley waves in the borehole is primarily caused by fractures intersecting the borehole. Additionally, the fluid flowing into the permeable fractures contributes to the attenuation of reflected Stoneley waves. Conversely, when the formation is consolidated and without fractures, the attenuation is minimal. Generally, the attenuation of the Stoneley wave increases with the degree of fracturing (Xiang et al., 2015).

In this study, most of the fractures in the Asmari carbonates have high dip angles, and these steeply (high dip) angled fractures significantly influence the energy attenuation of the Stoneley wave. Therefore, analyzing variations in Stoneley wave energy can provide valuable insights for detecting fracture zones (Zaree et al., 2016). Various dip angles of fractures can be identified through a comprehensive analysis of the full waveforms captured by DSI tools.

The Stoneley wave is dispersive, meaning its energy decreases as it moves radially away from the interface between the borehole and the

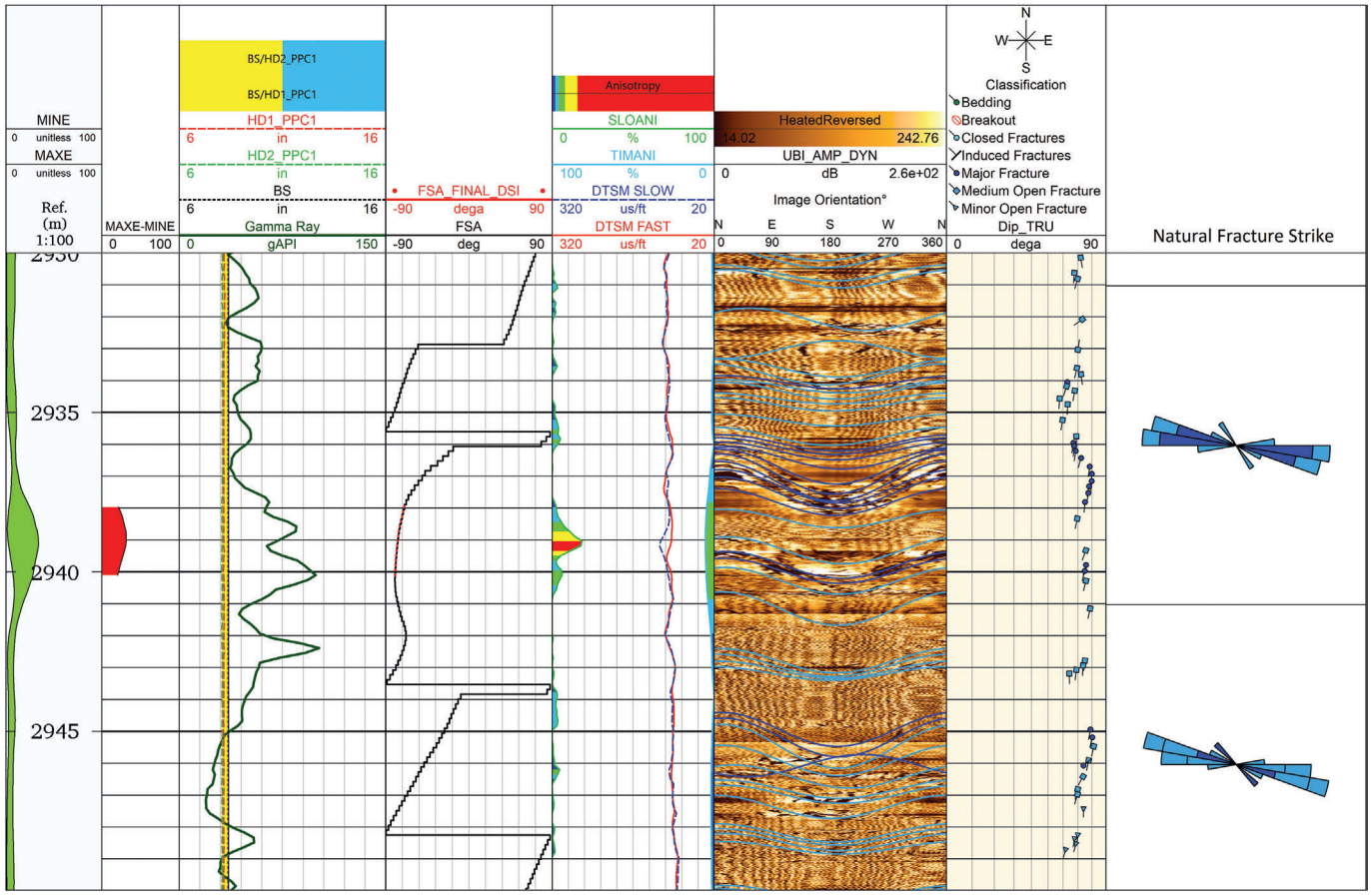

Fig. 13. Dipole sonic anisotropy with the associated acoustic borehole image [2930–2945 m].

surrounding formation. When open fractures intersect the borehole, the Stoneley wave experiences attenuation and generates reflected waves at the discontinuity between the fracture and the borehole wall. An analysis of the reflection and attenuation of the Stoneley waveform is performed, and both sets of results are utilized as input for a combined fracture aperture inversion (Brie et al., 1998b). This inversion process checks for consistency between the up-going and down-going reflections, as well as the transmission coefficient (the inverse of attenuation) while considering factors such as fracture dip and fracture density.

Sharp lithology boundaries with contrasting acoustic impedance can lead to Stoneley reflections. Likewise, washouts and borehole rugosity may contribute to the attenuation of Stoneley waves. To account for these borehole factors, a forward model is utilized to predict responses, which are then compared to the measured data (Tezuka et al., 1997).

The analysis of Stoneley and ultrasonic images is presented in Fig. 11. To identify existing fractures and their respective apertures, we performed inversions of both the transmission and reflection coefficients. The waveforms generated using the Tezuka model were based on the caliper response and elastic moduli. We computed the modelled reflection and transmission coefficients to illustrate the response of the Stoneley wave to borehole irregularities. Additionally, we calculated the elastic Stoneley slowness. A comparison of the measured Stoneley slowness (DTST) versus the modelled Stoneley slowness (DTST_STM) is shown in (Fig. 11, track 2), with the differences indicated by orange shading.

The computed transmission coefficients throughout the fractured intervals are significantly less than 1 (Fig. 11, Track 2). There are substantial differences in the Stoneley slowness (DTST and DTST_STM), with variations as low as 10 μs/ft (Fig. 11, Track 1). The reflection coefficients are quite minimal, typically under 0.05 in most intervals, and remain below 0.1 between depths of 2917 and 2919 m. This confirms that the response to a highly dipping fracture intersecting the borehole is primarily influenced by attenuation (Fig. 11, Tracks 3 and 4). The computed fracture apertures from the Stoneley data range from 0.05 to 0.15 inches (Fig. 11, Track 5).

5. Consistency with borehole images

Borehole imaging is a well-established technique that has been used since the mid-1980s to determine fracture types and the current stress direction in vertical wellbores (Fordjor et al., 1983). Figures 12–16 illustrate comparisons of sonic anisotropy, natural fractures, drilling-induced fractures, and borehole breakout. Natural fractures with wider apertures and high density are observed between depths of 2884–2895 m, 2903–2912 m, and 2937–2940 m. In contrast, fractures with smaller apertures can be found at depths of 2944–2948 m, 2952–2967 m, and 3223–3237 m. Borehole breakouts are identified at depths of 3280 m, 3284 m, 3295–3315 m, 3320 m, and 3325–3335 m in the acoustic image. Additionally, a few induced fractures are evident at depths of 2884 m and 2905–2908 m. At the same intervals, there are also indications of shear anisotropy. The representative slowness dispersion plots, shown in Figs. 8–10, exhibit characteristic dispersion curves for fast and slow shear waves typical for natural fractures, breakouts, and induced fractures. The fast shear azimuth is aligned with the direction of higher fracture intensity in the upper interval, while the lower interval aligns with the maximum horizontal stress direction given by breakouts on the image log. Further details are discussed below:

Natural open fractures are identified in the acoustic image (UBI) with various orientations. The UBI image indicates that open fractures are oriented in the NW-SE, WNW-ESE, and E-W directions between 2880 and 2895 m. However, the strike of fractures changes to the N-S

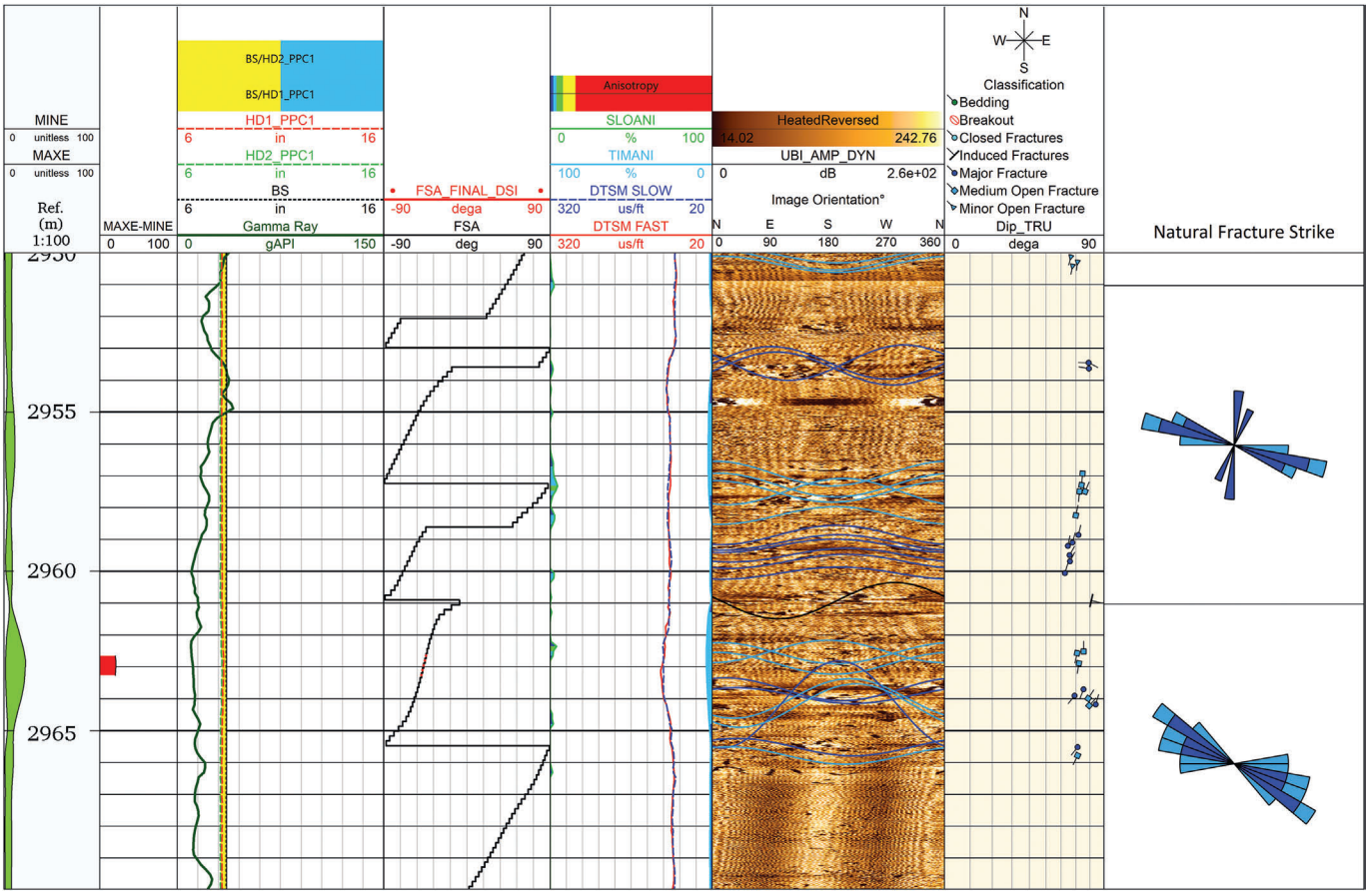

Fig. 14. Dipole sonic anisotropy with the associated acoustic borehole image [2950–2965 m].

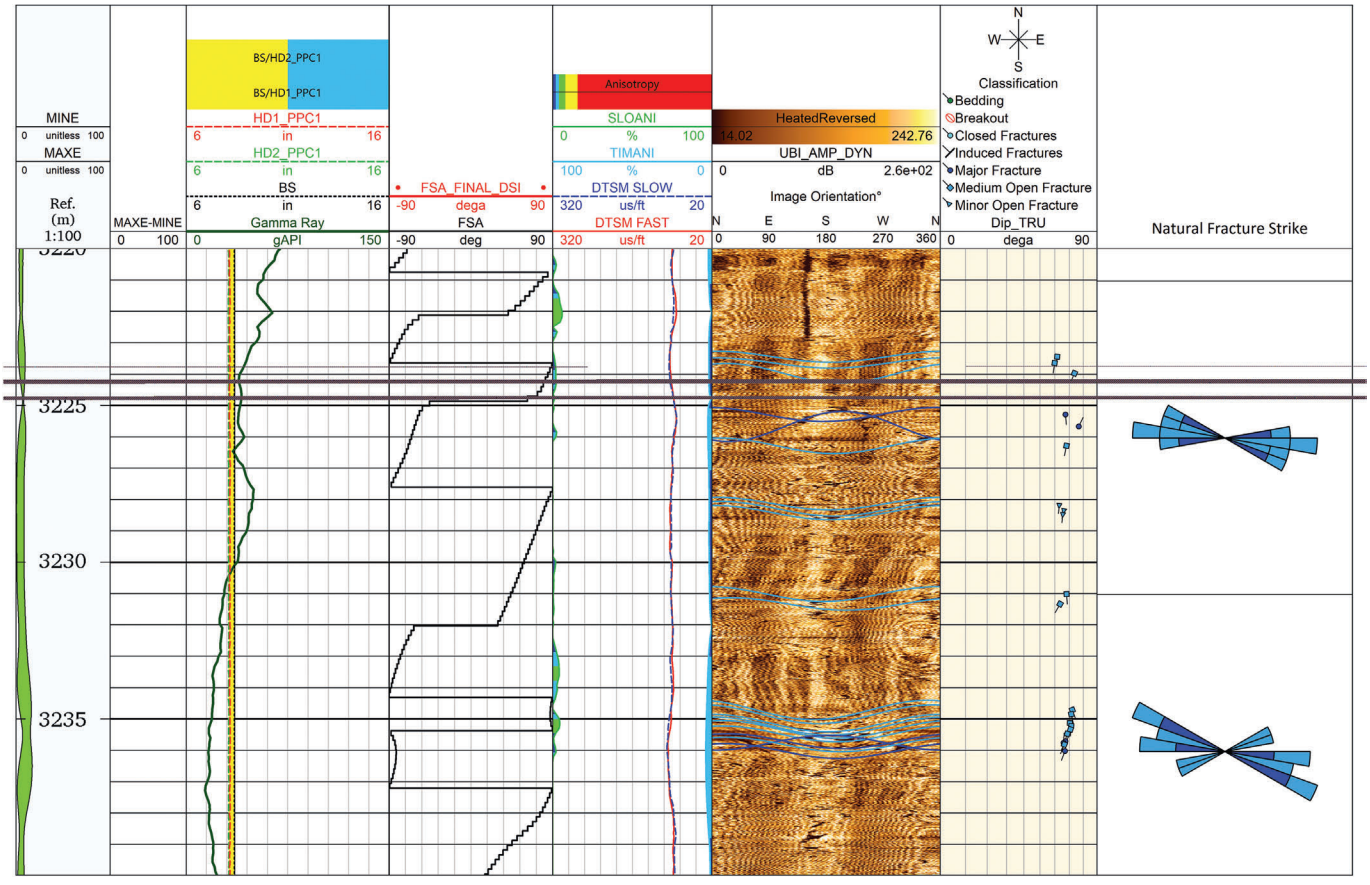

Fig. 15. Dipole sonic anisotropy with the associated acoustic borehole image [3220–3240m].

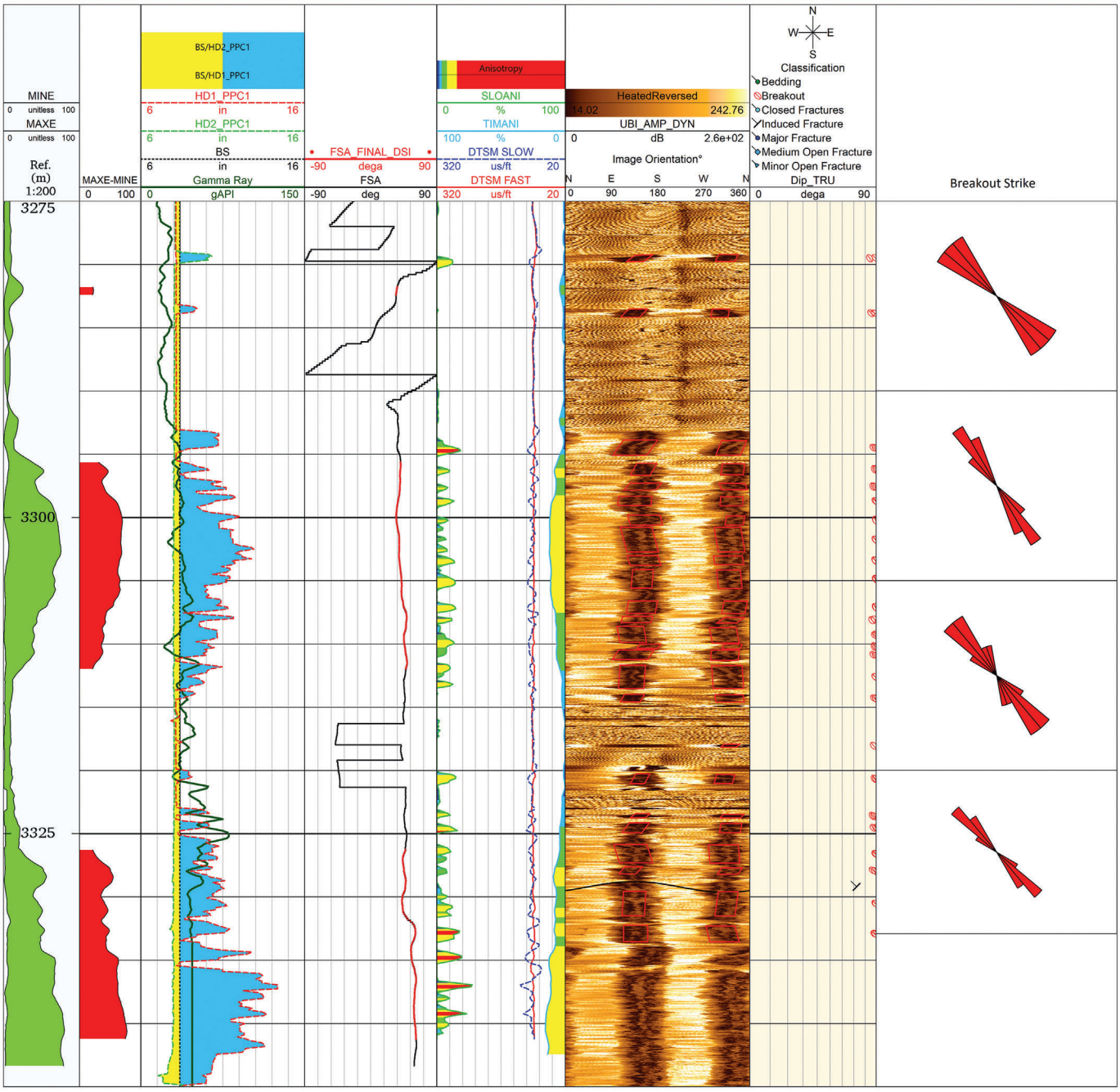

Fig. 16. Dipole sonic anisotropy with associated acoustic borehole image in track 6. Borehole breakouts are noted on the image.

direction (N10W-S10E) from 2900 to 2910 m, and then shifts back to NW-SE from 2912 to 2915 m (Fig. 12). This variation aligns with the results of anisotropy testing and the fast shear azimuth.

Fig. 12 illustrates the changes in the fast shear azimuth across these intervals. The fast shear azimuth direction is approximately N55°W to N70°W between 2884 and 2895 m. It then changes to N-S to N10°W at 2902–2910 m, and finally to N20°W to N30°W from 2910 to 2912 m. This azimuth change corresponds with the fracture orientations observed in these intervals (Fig. 12). Very few induced fractures were identified at the bottom, representing (reflecting) the NNE-SSW direction.

Fig. 13 illustrates another interval from 2937 to 2940 m with strong anisotropy. The fast shear azimuth is oriented at N70°W. The observed dispersion curves (Fig. 9) also reflect the natural fracture pattern, showing separated fast and slow shear curves at low frequencies (1–4 kHz). This change in azimuth aligns with the fracture orientation in this interval, which ranges from N70°W to E-W. Additionally, there is a smaller interval from 2962 to 2964 m that exhibits slow to medium anisotropy. The fast shear azimuth in this section is oriented at N45°W (Fig. 14), which is consistent with the fracture orientation observed in this interval.

The interval from 3225 to 3240 m shows low to medium anisotropy, with the fast shear azimuth oriented from N70°W to E-W (Fig. 15). This is consistent with the fracture orientation at this interval, which is WNW-ESE.

In the bottom interval, from 3279 to 3340 m, borehole breakouts with clear traces-characterized by dark bands of low reflectance were observed in UBI images. These breakouts indicate a minimum horizontal stress orientation ranging from N30W-S30E to N60W-S60E at the well location (Fig. 16). Consequently, the orientation of the maximum in-situ stress

near the wellbore is approximately N30E-S30W to N60E-S60W. The breakouts have been correlated with fast-shear azimuth measurements, which are oriented between N35E-S35W and N50E-S50W, indicating the direction of maximum horizontal stress (Fig. 16). Thus, the sonic anisotropy supports the same direction for maximum horizontal stress.

6. Conclusion

- This paper presents a robust methodology for accurately estimating stress direction from cross-dipole sonic data. The proposed qualification scheme for stress direction follows a similar trend observed in UBI image analysis, reinforcing its reliability.
- The analysis of shear wave anisotropy and the UBI image log complement one another and enhance confidence when both are utilized together.
- Dispersion analysis is a crucial tool for ensuring that the observed anisotropy stems directly from stress imbalance, fracturing or layering. This analysis not only validates slowness of anisotropy, but also helps determine the dominant mechanism responsible for anisotropy. This paper illustrates these concepts through several examples of dispersion curves from the Asmari and Pabdeh Formations, underscoring the effectiveness of this approach.
- The anisotropy analysis conducted using DSI data from the studied well identified five main intervals exhibiting formation anisotropy, with the maximum difference between the minimum and maximum energy observed. Notably, the intervals from 2884 to 2912 m and 3290–3340 m displayed higher anisotropy, attributed to the high fracture density and the presence of chevron patterns calculated from the Stoneley wave. Furthermore, the UBI image log revealed only a limited number of induced fractures. Impressively the UBI data uncovered 25 breakouts, which were distinctly visible in the lower section of this well, highlighting the complexity and potential of the formation.
- The analysis of the sonic data, alongside complementary image logs, indicates that the anisotropy observed in the upper intervals (2880–2895 m, 2902–2912 m and 2937–2940 m) is attributed to intrinsic fractures. Moreover, the fast shear azimuth reflects the modified fracture strike at these intervals, a finding that has been corroborated by the UBI image results.
- The orientation of the maximum stress in the Qaleh-Nar Oilfield was determined using the DSI tool and compared with the maximum stress direction found in the UBI Image log. Analysis of UBI data related to over 25 breakouts in the bottom interval indicates that the direction of maximum stress ranges from N30E-S30W to N60E-S60W. Additionally, the fast shear azimuth at the bottom interval is directed NE-SW, which is orthogonal to the breakout direction of NW-SE observed in both the DSI caliper and acoustic Image log. This suggests a maximum stress direction between N35E-S35W and N50E-S50W, which aligns with the maximum stress identified in the Zagros region.
- The findings of this study indicate that without an image log, a dipole sonic log can be relied upon to identify the nature of fractures and perform stress analysis.

CRediT authorship contribution statement

Maziar Torkaman: Software, Resources, Project administration. **Soheila Bagheri:** Writing – review & editing, Writing – original draft, Validation, Software, Conceptualization. **Mahdi Rastegarnia:** Validation, Supervision, Formal analysis, Data curation, Conceptualization.

Declaration of competing interest

The authors declare that they have no known competing financial interests or personal relationships that could have appeared to influence the work reported in this paper.

Acknowledgements

This study is based on the master's dissertation of the first author in the field of Petrophysics and has received approval from the Ethics Committee of Tehran University. The authors express their sincere gratitude to NISOC Company for providing data and allowing publication of these findings, and to the University of Tehran for its support in facilitating this research.

References

Alford, R.M., 1986. Shear data in the presence of azimuthal anisotropy". 56th Annual International Meeting, SEG, Expanded Abstracts, pp. 476–479.
Al-Adani, N., Alkhatib, H., 2009. The reality of borehole fracture propagation into the reservoir formation. SPWLA 50th Annual Logging Symposium, the Woodlands, Texas. June, SPWLA-2009-14997.
Almalki, M., Harris, B., Dupuis, J.C., 2013. Multifrequency full-waveform sonic logging in the screened interval of a large-diameter production well. Geophysics 78 (5).
Bakku, S.K., Fehler, M., Burns, D.R., 2012. Fracture Characterization from Attenuation of Stoneley Waves Across a Fracture. SEG Technical Program Expanded Abstracts.
Brie, A., Endo, D.L., Johnson, D.L., Pampuri, F., 1998. Quantitative formation permeability evaluation from stoneley waves. SPE Annual Technical Conference & Exhibition. New Orleans, Louisiana.
Burridge, R., Sinha, B.K., 1996. Inversion for formation shear modulus and radial depth of investigation using borehole flexural waves. 66th Ann. International. Mtg., Soc. Exp. Geophys., Expanded Abstracts 158–161.
Cheng, C.H., 2015. Can we trust the shear wave log? Lead. Edge 34 (3), 278–284.
Das, S., Nguyen, V.H., Asadi, S., Nathesan, N., Jamil, A., Milan, H., Chandrakant, A.A., Salleh, F.A., 2021. Integrated analysis of acoustic images and shear wave anisotropy used for geomechanical modelling in a tight sand oil reservoir. SPE/AAPG/SEG Asia Pacific Unconventional Resources Technology Conference.
Donald, A., Bratton, T.R., 2006. Advancement in acoustic technique for evaluating natural fractures. SPWLA 47th Annual Logging Symposium, Mexico, 4–7 June.
Donald, J.A., Prioul, R., Lei, T., Sinha, B., 2013. Stress characterization in deep boreholes using acousto-elasticity. In: Book: Rock Characterization, Modelling and Engineering Design Methods, pp. 309–314.
Donald, J.A., Wielemaker, E.J., Karpfinger, F., Gomez, F., Liang, X., Tingay, M., 2015. Qualifying stress direction from borehole shear sonic anisotropy. Presented at the 49th US Rock Mechanics/Geomechanics Symposium Held in San Francisco. CA, USA.
Ellis, D.V., Singer, J.M., 2007. Well Logging for Earth Scientists, second ed. New York.
Esmersoy, C., Koster, K., Williams, M., Boyd, A., Kane, M., 1994. Dipole shear anisotropy logging, 64th annual internat. Meet. Soc. Exp. Geophys. 1139–1142.
Esmersoy, C., Boyd, A., Kane, M., Denoo, S., 1995. Fracture and Stress Evaluation Using dipole-shear Anisotropy Logs: SPWLA 36th Ann. Meet.
Fang, X., Cheng, A., Fehler, M.C., 2015. Investigation of borehole cross-dipole flexural dispersion crossover through numerical modelling. Geophysics 80 (1), D75–D88.
Fordjor, C.K., Bell, J.S., Gough, D.I., 1983. Breakouts in Alberta and stress in the north AmericanPlate. Can. J. Earth Sci. 20, 1445–1455.
Franco, J.L.A., De, G.S., Renlie, L., Williams, S., 2006. Sonic investigations in and around the borehole. Oilfield Review (Spring) 14–33.
Habibnia, B., Vallipour, O., Alipour, M., 2021. Geochemical evaluation of oils from the asmari reservoir of the qale-nar oilfield: implication for field-scale reservoir compartmentalization. Iran. J. Oil Gas Sci. Technol. 10 (No.4), 68–84.
Hornby, B.E., Johnson, D.L., Winkler, K.W., Plumb, R.A., 1998. Fracture evaluation using reflected Stoneley-wave arrivals. Geophysics 54 (No.19), 1274–1288.
Irofti, D., Ifrene, G., Cheddad, F.A., Djemai, S., 2023. Integrating Borehole Imaging and Full Waveform Dipole Sonic Data to Estimate Fracture Porosity in Tight Formations: a Workflow for Accurate Characterization of Natural Fractures. AAPG Rocky Mountain Section Meeting. Bismarck, North Dakota, June 4–6.
Jamilpour, M., Mahboubi, A., Moussavi-Harami, R., Khanehbad, M., Hooshmand-Koochi, H., 2024. The new approach to establish a better match between obtained electrofacies and hydraulic flow units for Oligo-miocene reservoir rocks, north of dezful embayment, SW Iran. J. Pet. Explor. Prod. Technol. (14), 941–973.
Kimball, C.V., Marzetta, T.L., 1986. Semblance processing of borehole acoustic array data. Geophysics 49 (3), 274–281.
Lei, T., Michiko, H., Donald, A., Endo, T., 2021. Robust sonic log tracking using a multi-resolution approach. SPWLA 62nd Annual Logging Symposium, 17–20 May.
Mahmood, T., MacPherson, K.A., 2014. Differentiation of natural vs. drilling induced fractures in shale gas Wells using borehole Images– critical for determination of In-situ stress. AAPG Shale Gas Conference. UAE, Dubai, pp. 21–24. Sep.
Mao, 1987. Shear wave transducer for stress measurements in boreholes. U.S. Patent 4.
Motiei, H., 1995. Petroleum Geology of Zagros, vol. 1. Geological Survey of Iran Publication, p. 589.
Mueller, M.C., Boyd, A., Esmersoy, C., 1994. Case Studies of the Dipole Shear Anisotropy Log. SEG Technical Program Expanded Abstracts, pp. 1143–1146.
Pistre, V., Kinoshita, T., Endo, T., Schilling, K., Pabon, J., 2005. A modular wireline sonic tool for measurements of 3D (azimuthal, radial, and axial formation acoustic properties. SPWLA 46th Annual Logging Symposium. New Orleans, Louisiana, 26–29 June.
Plona, T.J., Kane, M.R., Sinha, B., Walsh, J., 2002. Evaluating stress-induced anisotropy and mechanical damage from cross-dipole sonic data using dispersion analysis. SPE/ISRM 78233 Rock Mechanics Conference, Texas, 20–23 October.

Plona, T., Endo, T., Wielemaker, E., Walsh, J., Yamamoto, H., 2006. Slowness-Frequency-Projection Logs: a QC for Accurate Slowness Estimation and Formation Property Identification. SEG Technical Program Expanded Abstracts, pp. 334–338. https://doi.org/10.1190/1.2370227.

Plumb, R.A., Hickman, S.H., 1985. Stress-induce borehole elongation: a comparison between the four-arm dipmeter and the borehole televiewer in the auburn geothermal well. J. Geophys. Res. 90 (B7), 5513–5521.

Prioul, R., Donald, A., Koepsell, R., Marzouki, A., Bratton, T., 2007. Forward modeling of fracture-induced sonic anisotropy using a combination of borehole image and sonic logs. Geophysics 72 (4), 135–147.

Razavi Pash, R., Sarkarinejad, K., Ghoochaninejad, H.Z., Motamedi, H., Yazdani, M., 2020. Accommodation of the different structural styles in the foreland fold-and-thrust belts: northern dezful embayment in the zagros belt, Iran. Int. J. Earth Sci. 109 (No.3), 959–970.

Rezaeeparto, K., Fazli, L., Parham, S., 2024. Reservoir quality controlling factor of theAsmari reservoir in an oil field in dezful embayment, SW Iran. J. Geol. 14, 259–278.

Sinha, B.K., Kostek, S., 1996. Stress-induced azimuthal anisotropy in borehole flexural waves. Geophysics 61 (6), 1899–1907.

Sinha, B.K., Bratton, T., Cryer, J., Nieting, S., Ugueto, G., Bakulin, A., Hauser, M., 2008. Estimation of near-wellbore alteration and formation stress parameters from borehole sonic data. SPE Reservoir Eval. Eng. 11 (3), 478–486.

Tang, X.M., Cheng, N.Y., Cheng, C.H., 1999. Identifying and estimating formation stress from borehole monopole and cross-dipole acoustic measurements: 40Th annual meeting. Society of Professional Well Log Analysts, Transactions.

Tang, X.M., Wang, T., Patterson, D., 2002. Multipole Acoustic logging-while-drilling: 72Nd Annual International Meeting. SEG, Expanded Abstracts, pp. 364–367.

Tezuka, K., Cheng, C.H., Tang, X.M., 1997. Modeling of low-frequency Stoneley-wave propagation in an irregular borehole. Geophysics 62, 1047–1058.

Wang, S., Wang, G.W., Li, D., Wu, X.N., Chen, X., Wang, Q.Q., Cao, J.T., Zhang, Y.L., 2022. Comparison between double caliper, imaging logs, and array sonic log for determining the in-situ stress direction: a case study from the ultra-deep fractured tight sandstone reservoirs, the Cretaceous bashijiqike formation in Keshen8 region of kuqa depression, tarim basin, China. Pet. Sci. 19, 2601–2617.

Winkler, K.W., Sinha, B.K., Plona, T.J., 1998. Effect of borehole stress concentration on dipole anisotropy measurements. Geophysics 63, 11–17.

Wood, D.A., 2024. Expanding role of borehole image logs in reservoir fracture and heterogeneity characterization: a review. Adv. Geo-Energy Res. 12 (3), 194–204.

Xiang, M., Wang, Z.W., Liu, J., 2015. Extracting array acoustic logging signal information by combining fractional fourier transform and choi–williams distribution. Appl. Acoust. 90, 111–115.

Zakharova, N.V., Goldberg, D.S., 2015. Analysis of shear-wave Anisotropy in Upper Oceanic Crust. Proceeding of Integrated Ocean Drilling Program, Tokyo, p. 335. https://doi.org/10.2204/iodp.proc.335.202.2015. V.

Zaree, V., Riahi, M.A., Khoshbakht, F., Hemmati, H.R., 2016. Estimating fracture intensity in hydrocarbon reservoir: an approach using DSI data analysis. Carbonates Evaporites 31 (1), 101–107.

Zoback, M.D., 2007. Reservoir Geomechanics, first ed. Cambridge University Press, p. 505.

Zoback, M.D., Moos, D., Mastin, L., Anderson, R.N., 1985. Wellbore breakouts and in situ stress. J. Geophys. Res. 90 (B7), 5523–5530.